Inorganic Chemistry

pubs.acs.org/IC

Article

Dynamics of the Energy Transfer Process in Eu(III) Complexes Containing Polydentate Ligands Based on Pyridine, Quinoline, and Isoquinoline as Chromophoric Antennae

Albano N. Carneiro Neto,* Renaldo T.MouraJr, Luís D. Carlos, Oscar L. Malta, Martina Sanadar, Andrea Melchior,* Elfi Kraka, Silvia Ruggieri, Marco Bettinelli, and Fabio Piccinelli*

Cite This: *Inorg. Chem.* 2022, 61, 16333−16346

Read Online

ACCESS | Metrics & More | Article Recommendations | Supporting Information

ABSTRACT: In this work, we investigated from a theoretical point of view the dynamics of the energy transfer process from the ligand to Eu(III) ion for 12 isomeric species originating from six different complexes differing by nature of the ligand and the total charge. The cationic complexes present the general formula $[Eu(L)(H_2O)_2]^+$ (where L = bpcd^{2-} = *N*,*N*′-bis(2-pyridylmethyl)-*trans*-1,2-diaminocyclohexane *N*,*N*′-diacetate; bQcd^{2-} = *N*,*N*′-bis(2-quinolinmethyl)-*trans*-1,2-diaminocyclohexane *N*,*N*′-diacetate; and *biso*Qcd^{2-} = *N*,*N*′-bis(2-isoquinolinmethyl)-*trans*-1,2-diaminocyclohexane *N*,*N*′-diacetate), while the neutral complexes present the $Eu(L)(H_2O)_2$ formula (where L = PyC3A^{3-} = *N*-picolyl-*N*,*N*′,*N*′-*trans*-1,2-cyclohexylenediaminetriacetate; QC3A^{3-} = *N*-quinolyl-*N*,*N*′,*N*′-*trans*-1,2-cyclohexylenediaminetriacetate; and *iso*QC3A^{3-} = *N*-isoquinolyl-*N*,*N*′,*N*′-*trans*-1,2-cyclohexylenediaminetriacetate). Time-dependent density functional theory (TD-DFT) calculations provided the energy of the ligand excited donor states, distances between donor and acceptor orbitals involved in the energy transfer mechanism (R_L), spin-orbit coupling matrix elements, and excited-state reorganization energies. The intramolecular energy transfer (IET) rates for both singlet-triplet intersystem crossing and ligand-to-metal (and vice versa) involving a multitude of ligand and Eu(III) levels and the theoretical overall quantum yields (ϕ_{ovl}) were calculated (the latter for the first time without the introduction of experimental parameters). This was achieved using a blend of DFT, Judd−Ofelt theory, IET theory, and rate equation modeling. Thanks to this study, for each isomeric species, the most efficient IET process feeding the Eu(III) excited state, its related physical mechanism (exchange interaction), and the reasons for a better or worse overall energy transfer efficiency (η_{sens}) in the different complexes were determined. The spectroscopically measured ϕ_{ovl} values are in good agreement with the ones obtained theoretically in this work.

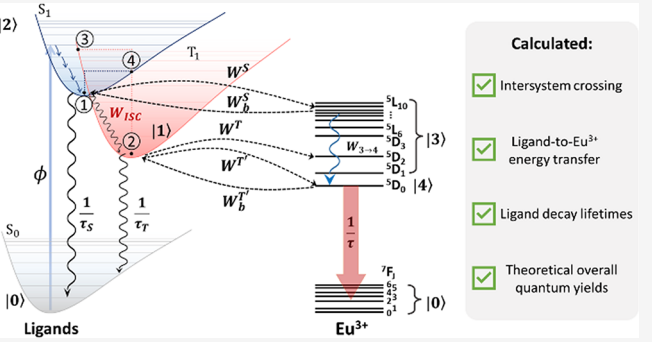

INTRODUCTION

The nonradiative intramolecular energy transfer (IET) process (also called *antenna effect*) is broadly exploited to increase the brightness of luminescent metal complexes, in particular for trivalent lanthanide ions[1] when, for example, these molecules are employed as optical probes for imaging[1−4] and luminescent sensing.[5−14] For such a class of compounds, brightness is defined as $B = \varepsilon \cdot \phi_{ovl} = \varepsilon \cdot \eta_{sens} \cdot \phi_{int}$, where ε is the molar absorption coefficient, ϕ_{ovl} is the overall quantum yield, i.e., the ratio of emitting/absorbed photons by the matrix/ligand, η_{sens} is the overall energy transfer efficiency, and ϕ_{int} is the intrinsic quantum yield, i.e., the ratio of emitting/absorbed photons upon direct excitation into a luminescent level of the lanthanide ion. Thus, to obtain high values of brightness, the combination of high ε, η_{sens}, and ϕ_{int} values is required ($\eta_{sens} = \eta_{ISC} \cdot \eta_{IET}$; where η_{ISC} and η_{IET} are the efficiency of the intersystem crossing (ISC)[15] and the IET processes, respectively). In this direction, one should avoid nonradiative processes, which negatively impact the ϕ_{int} value. These processes consist of (i) multiphonon relaxation (MPR) and (ii) backward energy transfer. They both may induce the nonradiative relaxation of the emitting levels, and the MPR process is particularly effective when high-energy vibrational modes (e.g., C−H, N−H, and O−H stretching) couple with the lanthanide electronic levels.[16−18] To obtain high ε and η_{sens} values, chromophoric ligands are employed, since they are capable, at the same time, of strong absorption of light (high ε

Received: July 4, 2022
Published: October 6, 2022

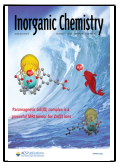

value, usually in the UV spectral range) and efficiently transfer the excitation energy to the lanthanide ion (high η_{sens} values).

From Dexter's theory,[19] nonradiative energy transfer processes from a donor (D, in the present case the ligand) to an acceptor (A, the lanthanide ion) can occur mainly by electric dipole−dipole, electric dipole−quadrupole, and exchange interactions. To optimize the efficiency of this process, the following requirements must be satisfied: (i) selection rules in the transitions of both D and A, (ii) short D−A distance (R_L), and (iii) strong spectral overlap of the emission band of D and the absorption band of A. In order to control all these features, precise knowledge of the D−A interaction is required. A complete and detailed description of the mechanism based on this interaction can be obtained by means of a combined experimental and theoretical study.[20] The photon absorption by D leads to an electron excitation that can result in $S_0 \rightarrow S_1$ or $S_0 \rightarrow T_1$ transitions. The S_1 state may nonradiatively transfer energy to a triplet excited state T_1 (a process known as intersystem crossing—ISC) or transfer energy to A (lanthanide ion), while the $S_0 \rightarrow T_1$ excitation involves a spin-forbidden transition and is much less probable that a triplet state will form. Ln(III)-based complexes favor ISC as a result of their more intense spin-orbit coupling (SOC),[21] which grows with the fourth power of the atomic number Z. Consequently, the theoretical methodology applied to account the D−A interaction requires the proper treatment of relativistic effects, which can be included by different methodologies, namely, the zero-order regular approximation (ZORA),[22,23] the Douglas−Kroll−Hess (DKH)[24,25] Hamiltonian, or the normalized elimination of the small component (NESC) method[26] and its updates and new implementations.[27−31] These methods offer different strengths and computational costs and are scalar relativistic corrections for the contraction of s- or p-orbitals and the expansion of d- or f-orbitals.

The $S_0 \rightarrow T_1$ and $S_1 \rightarrow T_1$ ISC at the scalar relativistic level is spin-forbidden, but SOC induces fast ISC by mixing singlet and triplet states, enabling these processes. Thus, accurate theoretical methods that can treat excited states with SOC in the presence of heavy elements are necessary for a precise description of the D−A interaction.[32] While different works in literature[33] approach the ISC for organic and d-metal complexes, few works[34] apply this type of calculation in lanthanide spectroscopy. However, the direct utilization of ISC for $S_1 \rightarrow T_1$ and $T_1 \rightarrow S_0$ nonradiative energy transfer rates on the calculation of the theoretical overall quantum yield (ϕ_{ovl}), as far as we know, is not found in the literature for a big set of Eu(III) excited states.

For this reason, in this paper, we present a detailed theoretical investigation, employing a blend of density functional theory (DFT), Judd−Ofelt theory, IET theory, and rate equation modeling, aimed to determine the relevant photophysical properties for 12 isomeric species originating from six different complexes previously designed and synthesized. These results, combined with an experimental spectroscopic study, mainly carried out previously by some of us,[10,12,35] give a detailed picture of the energy transfer mechanism in the different compounds. In particular, for Eu(III) complexes, we have determined (i) the nature and energy of the ligand levels (S_1 and T_1 donors) from DFT calculations; (ii) the D−A distances; (iii) the SOC matrix elements and reorganization energies for $S_1 \rightarrow T_1$ (λ_M) to calculate ISC rates (W_{ISC}); (iv) the reliable $S_0 \rightarrow S_1$ and $S_0 \rightarrow T_1$ (via SOC) dipole strengths to calculate S_0 and T_1 lifetimes; and (v) the contribution of dipole−dipole, dipole−quadrupole, and exchange mechanisms to the energy transfer process.

For the first time, the five points described above are used to perform simulations of the emitting-level populations from an appropriate rate equation model. Furthermore, these simulations permit the quantification of theoretical overall quantum yield (ϕ_{ovl}) without the introduction of experimental parameters. Thanks to this detailed study, we have been able to determine for each complex the main ligand and Eu(III) levels involved in the IET processes, the related physical mechanism, and the reasons for the better or worse overall energy transfer efficiency observed.

The deep knowledge of these photophysical properties is crucial in order to properly employ these classes of Eu(III) complexes as optical probes for the detection of important bioanalytes (i.e., citrate,[10] serum proteins,[11] hydrogen carbonate,[12] and lactate[13]).

THEORETICAL AND COMPUTATIONAL PROCEDURES

Computational Procedures. All molecular structures of the complexes were obtained by means of DFT calculations run in Gaussian 16 (version A.03).[36] The paramagnetic Eu(III) ion has been replaced by Y(III), which is a suitable substitute as shown in a previous work[13] and as can be deduced from the isostructural complexes with the analogous hexa-dentate ligands ethylenediaminetetraacetic acid (EDTA) and cyclohexanediaminetetraacetic acid (CDTA). In the crystal structures with these ligands, Y(III) and Eu(III) ions are nine-coordinated with EDTA (three water molecules bound) and eight-coordinated with CDTA (two bound waters).[37−39]

The functional B3LYP[40,41] was used with the 6−31+G(d) basis set for all ligand atoms and MWB28 pseudo-potential and the valence electron basis set for the metal ion.[42] Geometry optimizations were carried out at the DFT level with the solvent effect accounted by the polarizable continuum model (PCM) with the parameters for water.[43]

The excited states (T_1 and S_1) were obtained employing the time-dependent DFT approach (TD-DFT)[44] using the same procedure described for the geometry optimizations (B3LYP/MWB28(Y)/6−31+G(d)/PCM).

W_{ISC} was calculated using the Marcus−Levich[45−47] formalism. The values of λ_M were calculated utilizing the same procedure (B3LYP/MWB52(Eu)/6−31+G(d)/PCM) but selecting S_1 and T_1 excited states (from the TD-DFT calculations) for the geometry optimizations. The SOC matrix elements were calculated using SOC-TD-DFT[48] in ORCA5.0,[49] utilizing the B3LYP functional with ZORA[23] relativistic corrections. The recontracted ZORA-DEF2-TZVP[50] basis set for ligands and segmented all-electron relativistically contracted (SARC)-ZORA-TZVP for Eu atoms[51] were utilized. The calculations were done with the SARC/J auxiliary basis[51,52] and the resolution of the identity spin-orbit mean-field RI-SOMF[53] approximation. The calculated values of λ_M and SOC matrix elements, as well as the W_{ISC} rates, can be found in Table S15. Taking advantage of the SOC-TD-DFT approach, the dipole strengths of $S_0 \rightarrow T_1$ and $S_0 \rightarrow S_1$ excitations were obtained for calculating the S_1 and T_1 decay lifetimes (τ_S and τ_T, respectively) from Eq. S12.

Intramolecular Energy Transfer. The IET rates from organic ligands to Eu(III) ion were estimated taking into

https://doi.org/10.1021/acs.inorgchem.2c02330
Inorg. Chem. 2022, 61, 16333−16346

consideration the dipole−dipole (W_{d-d}), dipole−multipole (W_{d-m}), and exchange (W_{ex}) mechanisms:[20,54−57]

$$W_{d-d} = \frac{S_L(1-\sigma_1)^2}{(2J+1)G}\frac{4\pi}{\hbar}\frac{e^2}{R_L^6} \times \sum_\lambda \Omega_\lambda^{FED}\langle \psi' J'\left\| U^{(\lambda)} \right\| \psi J\rangle^2 F \quad (1)$$

$$W_{d-m} = \frac{S_L}{(2J+1)G}\frac{2\pi e^2}{\hbar}\sum_\lambda (\lambda+1)\frac{\langle r^\lambda\rangle^2}{(R_L^{\lambda+2})^2} \times \langle f\left\| C^{(\lambda)} \right\| f\rangle^2 (1-\sigma_\lambda)^2 \langle \psi' J'\left\| U^{(\lambda)} \right\| \psi J\rangle^2 F \quad (2)$$

$$W_{ex} = \frac{(1-\sigma_0)^2}{(2J+1)G}\frac{8\pi}{\hbar}\frac{e^2}{R_L^4}\langle \psi' J'\| S\| \psi J\rangle^2 \times \sum_m |\langle \phi| \sum_j \mu_z(j) s_m(j)|\phi^*\rangle|^2 F \quad (3)$$

where R_L is the donor−acceptor state distance and Ω_λ^{FED} (ESI) are the intensity parameters (or Judd−Ofelt parameters) by the forced electric dipole (FED) mechanism.[58,59] The simple overlap model[60,61] was employed to calculate these quantities through the JOYSpectra web platform.[62] The values of the squared reduced matrix elements $\langle \psi' J'\| U^{(\lambda)}\| \psi J\rangle^2$ were taken from Carnall et al.,[63] whereas the $\langle \psi' J'\| S\| \psi J\rangle$ matrix elements were calculated using free-ion wavefunctions in the intermediate coupling scheme.[64,65] The values of $\langle \psi' J'\| S\| \psi J\rangle$ for allowed ($|\Delta J| = 0$ or 1) $^7F_0 \rightarrow {}^5D_1$, $^7F_1 \rightarrow {}^5D_0$, $^7F_1 \rightarrow {}^5D_1$, $^7F_1 \rightarrow {}^5D_2$, and $^7F_1 \rightarrow {}^5G_2$ acceptor transitions are reported in Table S2 in the ESI. S_L is the dipole strength of the ligand transition involved in IET (10^{-36} and 10^{-40} (esu)$^2 \cdot$ cm^2 for S_1 and T_1, respectively[20]), $\langle r^\lambda\rangle$ are the 4*f* radial integrals,[66] G is the ligand state degeneracy ($G = 1$ or 3 for S_1 or T_1, respectively), $\langle f\| C^{(\lambda)}\| f\rangle$ is the reduced matrix element of Racah's tensor operators,[67] and $(1-\sigma_k)$ (for $k = 1$ and 2) are the shielding factors, which have a relation with the overlap integrals between valence orbitals of the pair Ln−X (X as the ligating atom in the first coordination sphere).[57,68] The values of $(1-\sigma_k)$ for k= 4 and 6 can be found in ref 66. s_m (in eq 3) is the spin operator in the ligand, and μ_z is the dipole operator (z component); the value of the element matrix of these coupled operators is 10^{-36} (esu)$^2 \cdot$ cm^2.[20,69]

The F term in eqs 1−3 is the density of states (proportional to the spectral overlap) that considers the energy mismatch condition between donor (ligands) and acceptor states (Ln(III) ion).[20,54] F can be estimated by

$$F = \frac{1}{\hbar\gamma_D}\sqrt{\frac{\ln(2)}{\pi}}\, e^{-\left(\frac{\Delta}{\hbar\gamma_D}\right)^2 \ln(2)} \quad (4)$$

where Δ is the energy difference between the donor barycenter state and the lanthanide ion acceptor state ($\Delta = E_D - E_A$). γ_D is the bandwidth at half-height of the donor states (S_1 and T_1), assumed here to have a typical value of $\gamma_D = 3000$ cm^{-1} for both S_1 and T_1 states.[70,71]

The forward energy transfer rates (W) involving the Eu(III) ions as acceptors are calculated by the sum over eqs 1−3 in the same pathway:

$$W = W_{d-d} + W_{d-m} + W_{ex} \quad (5)$$

If Δ is negative, for a given energy transfer pathway, W must be multiplied by the energy barrier factor $\exp(\Delta/k_BT)$, where k_B is the Boltzmann constant and T is the temperature (considered to be 298.15 K in the present work). For example, consider that a given forward pathway $T_1 \rightarrow [{}^7F_0 \rightarrow {}^{2S+1}L_J]$ has $\Delta = -500$ cm^{-1}, then the total rate (eq 5) of this specific pathway should be multiplied by 0.09 (barrier factor). The barrier factor is not applied for the backward energy transfer $[{}^{2S+1}L_J \rightarrow {}^7F_0] \rightarrow T_1$ because $\Delta = 500$ cm^{-1}. In addition, depending on the Eu(III) initial state involved in the energy transfer pathway (e.g., $^7F_1$ in the $T_1 \rightarrow [{}^7F_1 \rightarrow {}^5D_1]$ pathway or $^7F_0$ in the $S_1 \rightarrow [{}^7F_0 \rightarrow {}^5L_6]$ pathway), W is multiplied by the thermal population fraction at room temperature (0.64 for $^7F_0$ and 0.33 for $^7F_1$).[65,72]

The IET rates from the ligands to the Eu(III) ion were calculated using both $S_0 \leftarrow S_1$ and $S_0 \leftarrow T_1$ decay transitions as energy donors localized in the ligands and a total of 32 energy transfer pathways involving $^7F_0$ and $^7F_1$ as initial states and $^5D_0$, $^5D_1$, $^5D_2$, $^5D_3$, $^5L_6$, $^5L_7$, $^5G_2$, $^5G_3$, $^5G_4$, $^5G_6$, $^5D_4$, $^5G_5$, $^5L_8$, $^5D_4$, $^5L_9$, and $^5L_{10}$ as final states at the Eu(III) ion. Consequently, 64 IET pathways were computed for each one of the 12 studied complexes, totalizing 768 IET rates analyzed (half of them are non-zero due to selection rules on the J quantum number[20]).

Rate Equations and Overall Emission Quantum Yield. Once the IET rates are determined, the system of rate equations constituted by coupled ordinary differential equations (ODEs) can be solved to determine the relative population of each level. The set of ODEs can be solved in the analytical form, which assumes that the system is in a steady-state regime (all derivatives equal to zero) and the ground levels are very little depleted. Thus, the population of the Ln(III) emitting level is given by analytical expressions.[20,65,73,74] On the other hand, the set of coupled ODEs can be solved by numerical methods through time propagation. This approach was adopted in this work.

The set of ODEs can be described as follows:[14,20,75]

$$\frac{dP_i(t)}{dt} = \sum_{j=1} W_{j\rightarrow i}P_j(t) - \sum_{j=1} W_{i\rightarrow j}P_i(t), \text{ with } i \neq j \quad (6)$$

where both summations run all levels of the system. P_i and P_j are the populations of the levels $|i\rangle$ and $|j\rangle$ and $W_{j\rightarrow i}$ and $W_{i\rightarrow j}$ are the energy transfer rates between these states. Thus, an N-level rate equation model can be described by a set formed by N-coupled ODEs. The appropriate set of rate equations, with their respective initial conditions, can be numerically solved using several methods such as fourth-order Runge−Kutta with fixed-step or adaptive-step size, Radau, and Adams−Bashforth, among others.[76] We adopted the Radau method[77] in the simulations since it was applied in other Ln-based complexes and provided very consistent results[14,78−83] with a low computational cost. Each simulation was done in a time interval from 0 to 10 ms with a step-size of 2 μs.

The solution of the rate equation model permits the estimation of the emitting level population P_E of the Ln(III) (e.g., $^5D_0$ of the Eu(III) ion), and consequently, the emission intensity $I = A_{rad}P_E$, where A_{rad} (Table S1) is the spontaneous emission coefficients, which can be calculated from the Judd−Ofelt intensity parameters.[20,58,59,62,63,84]

The overall quantum yield ϕ_{ovl} is defined by the ratio of the numbers of photons emitted and absorbed by the matrix/ligand,[1,20,85,86]

$$\phi_{ovl} = \frac{\text{number of photons emitted}}{\text{number of photons absorbed}} = \frac{A_{rad}P_E}{\phi P_0} \quad (7)$$

https://doi.org/10.1021/acs.inorgchem.2c02330
Inorg. Chem. 2022, 61, 16333−16346

where P_0 is the population of the ground level and ϕ is the pumping rate of the populations from this level (e.g., $S_0 \rightarrow S_1$ intra-ligand absorptions). The latter can be estimated by $\phi = \sigma\rho\lambda_{exc}/hc$, where σ is the absorption cross section of the ligand (in the order of $\sim 10^{-16}$ $cm^2 \cdot molecule^{-1}$),[87] ρ is the power density in units of watts per square centimeter, λ_{exc} is the excitation wavelength, h is Planck's constant, and c is the speed of light.[14,78,79,88]

EXPERIMENTAL MEASUREMENTS

The overall quantum yields ϕ_{ovl} for the complexes $[Eu(bisoQcd)(H_2O)_2]^+$ and $[Eu(isoQC3A)(H_2O)_2]$ were experimentally obtained by secondary methods described in the literature[89] by measuring the visible emission spectrum of quinine bisulfate in 0.5 M H_2SO_4 solution, a fluorescence quantum yield reference sample (ϕ_s = 54.6%). ϕ_{ovl} for the complexes is calculated by the equation $\phi_{ovl} = [(A_s \cdot F_u \cdot n^2)/(A_u \cdot F_s \cdot n_o^2)] \cdot \phi_s$, where the u subscript refers to unknown (the sample under investigation) and s to the standard, and other symbols have the following meanings: ϕ_s is the overall quantum yield of the reference sample, A is the absorbance at the excitation wavelength, F is the integrated emission area across the band, and n's are respectively the index of refraction of the solvent containing the unknown (n) and the standard (n_o) at the sodium D line and the temperature of the emission measurement (see ESI, Figures S16 and S17). The measurements were repeated three times, and the averaged value is provided.

RESULTS AND DISCUSSION

Structural and Thermodynamic Properties of the Complexes in Aqueous Solution. The chemical structures and the labels of the Eu(III) and Y(III) complexes described in this work are shown in Figure 1. The Eu(III) compounds were previously synthesized and spectroscopically characterized, and the Y(III) counterparts have been used exclusively as a computational structural model of the paramagnetic Eu(III) analogs, in view of the similar ionic radii of the two cations.[90,91]

For the sake of clarity, the investigated complexes have been divided into three groups, differing by the nature of the heteroaromatic ring: pyridine (group **I**), quinoline (group **II**), and *iso*quinoline (group **III**).

The protonation constants (log K) of the considered ligands are reported in Table 1. These values indicate that two fairly strong acidic and two weakly acidic sites are present. As previously discussed,[10−12,35] the values for the first protonation constants of the ligands are in agreement with those reported for tertiary amines (log $K \sim 6.9-10.7$, depending on the substituents),[92] suggesting that the first protonation constant can be assigned to an aliphatic amino group, as previously reported for CDTA.[93] The remaining protonation constants are ascribed to heteroaromatic (pyridine, quinoline, and isoquinoline) rings and acetate moieties.[10−12,35]

As for the speciation in aqueous solutions of the investigated complexes, at the physiological pH = 7.4, the ML species is largely predominant in all cases (>99%), with the exception of bpcd-based complexes for which a small amount (around 5%) of the neutral hydroxo $[Eu(bpcd)(OH)(H_2O)]$ complex was also detected.[35]

Because of the strong oxophilicity of the Ln(III) ions,[91] the stability constants (log β) for the triacetate ligands [PyC3A, QC3A, and *iso*QC3A] are higher than their diacetate analogues [bpcd, bQcd, and b*iso*Qcd, respectively]. Besides, the stability constants of the Eu(III) complexes with the quinoline- and isoquinoline-substituted ligands are lower than for their pyridine analogues (bpcd and PyC3A). This result could be due to a weaker interaction of the quinoline moieties with the metal ion with respect to the pyridine ones and to the increased steric hindrance. From the perspective of the biological applications, the values of log β appear promising, in particular for the triacetate-based ligands (PyC3A, QC3A, and *iso*QC3A) whose stability is close to that of macrocyclic ligands possessing a similar coordination ability and already employed in molecular imaging applications (i.e., DO3A derivatives with log β values in the 18−21 range[94]).

Molecular models obtained from DFT calculations on the Y(III) counterparts (complexes **A**−**F**) of Eu(III) complexes show that Y(III) is in all cases eight-fold coordinated with six donor atoms belonging to the ligand and two oxygen atoms to coordinated water molecules, the general formula being $[Y(L)(H_2O)_2]$, as illustrated in Figure 1. As two different coordination geometries, differing by the stereochemistry of the sp^3 nitrogen atoms, are possible for each ligand (Figure 2), DFT calculations are performed on 12 species, whose labeling is reported in Table 2 while the minimum energy structures are shown in Figure 3.

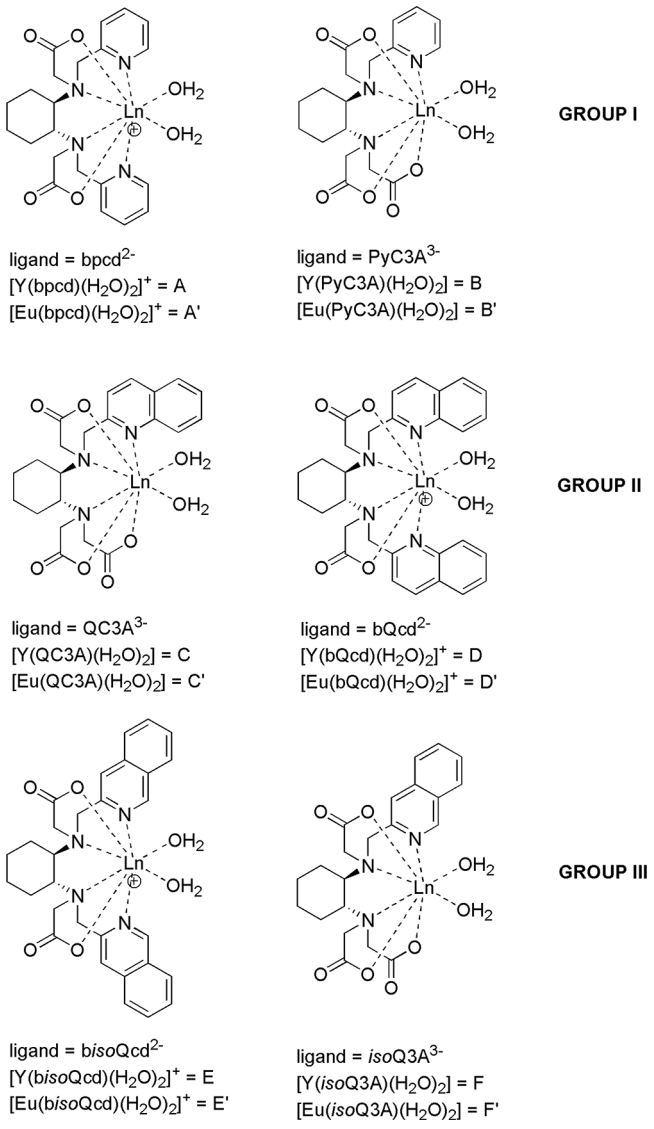

Figure 1. Chemical structures of the Ln(III) complexes studied in this work. Ln = Y(III) and Eu(III).

https://doi.org/10.1021/acs.inorgchem.2c02330
Inorg. Chem. 2022, 61, 16333−16346

Table 1. Protonation Constants (log K_j) and Formation Constants (log β) for the Complexes with Eu(III) Described in This Work at 298.15 K and μ = 0.1 M NaCl[a]

reaction	bpcd[b]	PyC3A[c]	bQcd[c]	QC3A[c]	b*iso*Qcd[d]	*iso*QC3A[e]	CDTA[f]
			log K_j				
L + H ⇆ HL	9.72	10.26	9.37	10.53	9.27	9.43	9.43
HL + H ⇆ H_2L	5.87	6.33	5.85	6.29	5.86	7.37	6.01
H_2L + H ⇆ H_3L	2.94	3.67	3.46	3.60	3.43	3.32	3.68
H_3L + H ⇆ H_4L	2.22	2.01	1.79	2.81	1.62	2.16	2.51
			log β				
L + Eu ⇆ EuL	11.19	15.68	9.97	12.55	10.53	14.63	19.60

[a]Additional protonation and formation constants data of the analog CDTA ligand are also reported for comparison. Charges are omitted for simplicity. [b]Data from ref 35. [c]Data from ref 12. [d]Data from ref 11. [e]Data from ref 10. [f]CDTA: cyclohexanediaminetetraacetic acid; data taken from ref 95.

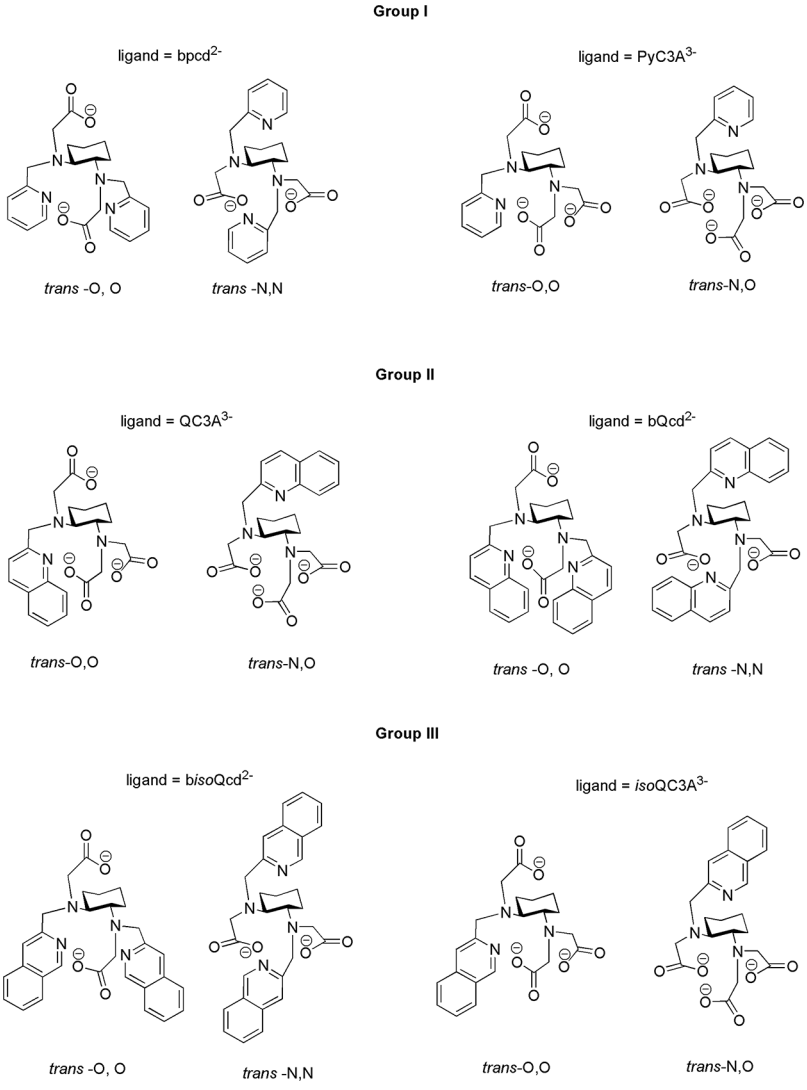

Figure 2. Possible coordination geometries of the ligands in this paper.

From a structural point of view, the increase in steric crowding when passing from pyridine- to the quinoline-substituted ligands is clearly seen upon inspection of the structures shown in Figure 3. This steric increase may reflect the change in Judd−Ofelt intensity parameters, more precisely in the general interpretation that Ω_4 and Ω_6 parameters correlate with the rigidity of a compound.[96,97] Accordingly, an increase in the average $\bar{\Omega}_4$ and $\bar{\Omega}_6$ (Table S1) between groups is observed: $\bar{\Omega}_{4,6}$(**I**) < $\bar{\Omega}_{4,6}$(**II**) < $\bar{\Omega}_{4,6}$(**III**).

From the resulting bond distances (Table 3), it emerges that the substitution of pyridine by quinoline or isoquinoline has nearly no effect on the Y(III)−$O_{acetate}$ bonds (average variation, ΔPy → Q ∼ −0.001 and + 0.005 Å for the di- and tri-acids, respectively), and the Y(III)−N_{amine} distances are marginally affected (ΔPy → Q ∼ −0.019 and − 0.006 Å). It can also be noted that Y(III)−O_{water} bonds are slightly longer in the pyridine triacid isomers as could be expected on the basis of the decreased charge on the metal ion, while in the quinoline

https://doi.org/10.1021/acs.inorgchem.2c02330
Inorg. Chem. 2022, 61, 16333−16346

Table 2. Labels, Group Membership, and Formula of the Complexes in This Paper

complex	isomer	formula	group
A	1	*trans-O,O*-[Y(bpcd)$(H_2O)_2$]$^+$	I
	2	*trans-N,N*-[Y(bpcd)$(H_2O)_2$]$^+$	
A′	1′	*trans-O,O*-[Eu(bpcd)$(H_2O)_2$]$^+$	
	2′	*trans-N,N*-[Eu(bpcd)$(H_2O)_2$]$^+$	
B	3	*trans-N,O*-[Y(PyC3A)$(H_2O)_2$]	
	4	*trans-O,O*-[Y(PyC3A)$(H_2O)_2$]	
B′	3′	*trans-N,O*-[Eu(Pyc3A)$(H_2O)_2$]	
	4′	*trans-O,O*-[Eu(PyC3A)$(H_2O)_2$]	
C	5	*trans-N,O*-[Y(QC3A)$(H_2O)_2$]	II
	6	*trans-O,O*-[Y(QC3A)$(H_2O)_2$]	
C′	5′	*trans-N,O*-[Eu(QC3A)$(H_2O)_2$]	
	6′	*trans-O,O*-[Eu(QC3A)$(H_2O)_2$]	
D	7	*trans-O,O*-[Y(bQcd)$(H_2O)_2$]$^+$	
	8	*trans-N,N*-[Y(bQcd)$(H_2O)_2$]$^+$	
D′	7′	*trans-O,O*-[Eu(bQcd)$(H_2O)_2$]$^+$	
	8′	*trans-N,N*-[Eu(bQcd)$(H_2O)_2$]$^+$	
E	9	*trans-O,O*-[Y(b*iso*Qcd)$(H_2O)_2$]$^+$	III
	10	*trans-N,N*-[Y(b*iso*Qcd)$(H_2O)_2$]$^+$	
E′	9′	*trans-O,O*-[Eu(b*iso*Qcd)$(H_2O)_2$]$^+$	
	10′	*trans-N,N*-[Eu(b*iso*Qcd)$(H_2O)_2$]$^+$	
F	11	*trans-O,O*-[Y(*iso*QC3A) $(H_2O)_2$]	
	12	*trans-N,O*-[Y(*iso*QC3A) $(H_2O)_2$]	
F′	11′	*trans-O,O*-[Eu(*iso*QC3A) $(H_2O)_2$]	
	12′	*trans-N,O*-[Eu(*iso*QC3A) $(H_2O)_2$]	

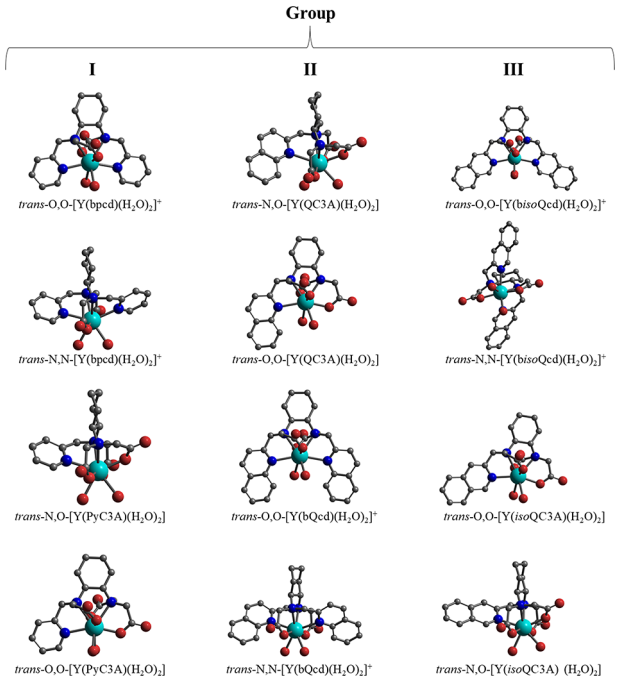

Figure 3. Group assignment, formula, and minimum energy DFT structure of the possible isomers of the Y(III) counterparts of the investigated Eu(III) complexes. Hydrogen atoms are removed for clarity.

complexes, they are only slightly affected. However, the most remarkable finding is that the average Y(III)−$N_{heterocycle}$ bond distance increases in the Py → *iso*Q→Q order. In the case of quinoline-based complexes, the increase of this bond distance is 0.11 Å with respect to the pyridine ligands (ΔPy → Q ∼ +0.11 Å), indicating the weaker interaction of quinoline with the metal ion; this possibly contributes to the drop of stability of the quinoline complexes compared to the pyridine analogues (on average ∼1.4 and 3.4 log units for the di- and tri-acetate ligands). However, it is expected that quinoline also has a notable impact on the solvation properties of the complex, which often have a strong influence on the stability.

Spectroscopic Properties of the Complexes. As reported in Table 4, the experimental spectroscopic study on the Eu(III) complexes shows low to moderate intrinsic quantum yields (ϕ_{int} in the 5−10% range) for all compounds, which reflect the presence of MPR quenching, induced by water molecules in the proximity of the metal ion (hydration number q calculated by the Horrocks equation[98−100]), which is detrimental for the luminescence efficiency. This number, in the 2.5−2.8 range (Table 4), even if slightly larger than that found by DFT calculation (q = 2), is still in agreement with it. It must be pointed out that the q number is also sensitive to the presence of water in the outer coordination sphere of the metal ion. On the other hand, the presence of water molecules bound to Eu(III) is required to use these metal complexes as optical probes to sense biomolecules or bioanalytes. In fact, some of us reported how the displacement of this bound water by the target molecule is based on the optical sensing mechanism of important bioanalytes such as HCO_3^-,[12] citrate,[10] and bovine serum albumin (BSA).[11]

As for the overall quantum yield (ϕ_{ovl}), we noticed a significant drop in its value in the case of the quinoline- and isoquinoline-based complexes (group **II** and **III** molecules) due to a worse efficiency of the sensitization process (η_{sens}), which includes the ISC and the IET phenomena. η_{sens} is about 25% in the case of [Eu(b*iso*Qcd)$(H_2O)_2$]$^+$ (**9′** + **10′**) complexes (Table 4), corresponding to an overall quantum yield of around 1%. The reasons for this behavior will be discussed in detail in the next sections of the paper. Finally, upon excitation into the ligand absorption bands (Figure 4), the luminescence of Eu(III) is sensitized and the emission spectra of the related complexes are all compatible with an emitting ion located in a non-centrosymmetric site. As it is well known in this case, the $^5D_0 \rightarrow {}^7F_2$ hypersensitive transition dominates the spectra[101] (Figure 4). Nevertheless, the $^5D_0 \rightarrow {}^7F_4$ transitions are also very strong in comparison to $^5D_0 \rightarrow {}^7F_1$ (used as a reference), suggesting that the Eu(III) ion is in a distorted cubic symmetry.[102,103] The theoretical intensity parameters Ω_λ (Table S1) agree with the spectra in Figure 4.

Furthermore, all complexes exhibit a relatively strong $^5D_0 \rightarrow {}^7F_0$ transition (particularly in the case of quinoline-based complexes). This feature is compatible with an axial character of the Eu(III) point symmetry.[101] C_n, C_{nv}, and C_s are the only possible point symmetries in the presence of sizeable intensity of the $^5D_0 \rightarrow {}^7F_0$ transition,[104,105] even if the C_s symmetry can be ruled out due to the presence of the chiral ligand. The relatively high intensity of $^5D_0 \rightarrow {}^7F_0$ suggests that the studied compounds experience a strong *J*-mixing effect.[106−109]

Excited States of the Ligands. From TD-DFT calculations, donor energy levels (S_1 and T_1) were obtained together with their respective donor−acceptor distances, fundamental quantities used in eq 4 (Δ value in *F*) and eqs 1−3 (R_L), respectively.

Table 5 summarizes the calculated S_1 and T_1 energy positions, and Figures S1−S12 show the main compositions of these excited states. Once S_1 and T_1 states are both characterized as an electronic density displacement to the same portion in the compound (see unoccupied molecular

https://doi.org/10.1021/acs.inorgchem.2c02330
Inorg. Chem. 2022, 61, 16333−16346

Table 3. Selected Bond Distances (Å) of the Complexes in Table 2

group	formula (isomer)	Y−$O_{acetate}$	Y−N_{amine}	Y−$N_{heterocycle}$	Y−O_{water}
I	[Y(*trans-O,O* bpcd)$(H_2O)_2]^+$ (**1**)	2.262	2.550	2.525	2.448
	[Y(*trans-N,N* bpcd)$(H_2O)_2]^+$ (**2**)	2.292	2.610	2.503	2.492
	[Y(*trans-O,O* PyC3A)$(H_2O)_2$] (**3**)	2.286	2.568	2.550	2.474
	[Y(*trans-N,O* PyC3A)$(H_2O)_2$] (**4**)	2.300	2.595	2.546	2.539
II	[Y(*trans*-O,O QC3A)$(H_2O)_2$] (**5**)	2.286	2.574	2.654	2.458
	[Y(*trans-N,O* QC3A)$(H_2O)_2$] (**6**)	2.290	2.576	2.642	2.478
	[Y(*trans-O,O* bQcd)$(H_2O)_2]^+$ (**7**)	2.268	2.557	2.661	2.464
	[Y(*trans-N,N* bQcd)$(H_2O)_2]^+$ (**8**)	2.284	2.567	2.594	2.482
III	[Y(*trans-O,O biso*Qcd)$(H_2O)_2]^+$ (**9**)	2.262	2.577	2.526	2.451
	[Y(*trans-N,N biso*Qcd)$(H_2O)_2]^+$ (**10**)	2.283	2.565	2.614	2.463
	[Y(*trans-O,O iso*QC3A)$(H_2O)_2$] (**11**)	2.297	2.594	2.581	2.509
	[Y(*trans-N,O iso*QC3A)$(H_2O)_2$] (**12**)	2.297	2.579	2.553	2.471

Table 4. Experimental Intrinsic ϕ_{int}, Overall ϕ_{ovl} Quantum Yields (in %), and η_{sens} (in %) Reported for the Investigated Eu(III) Complexes[e]

group	complex	formula	ϕ_{int}	η_{sens}	ϕ_{ovl}	q
I	A′	[Eu(bpcd)$(H_2O)_2]^+$ (**1′** + **2′**)	10.0(1)[b]	61[b]	6.1(3)[b]	2.7(1)[a]
	B′	[Eu(PyC3A)$(H_2O)_2$] (**3′** + **4′**)	9.0(1)[b]	67[b]	6.0(3)[b]	2.7(1)[b]
II	C′	[Eu(QC3A)$(H_2O)_2$] (**5′** + **6′**)	9.9(1)[b]	40[b]	4.0(2)[b]	2.5(1)[b]
	D′	[Eu(bQcd)$(H_2O)_2]^+$ (**7′** + **8′**)	9.0(1)[b]	29[b]	2.6(3)[b]	2.8(1)[b]
III	E′	[Eu(*biso*Qcd)$(H_2O)_2]^+$ (**9′** + **10′**)	5.0(1)[c]	26	1.3(1)[d]	2.8(1)[c]
	F′	[Eu(*iso*QC3A)$(H_2O)_2$] (**11′** + **12′**)	5.4(1)[c]	40	2.2(2)[d]	2.8(1)[c]

[a]Ref 35. [b]Ref 12. [c]Ref 10. [d]The data were determined in this work by using the reference standard. [e]q is the calculated number of water molecules.

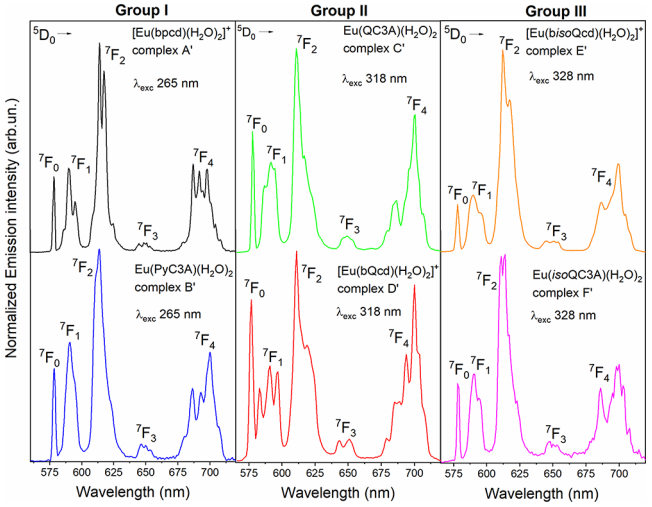

Figure 4. Room temperature luminescence emission spectra of the investigated Eu(III) complexes in aqueous solution (100 mM) upon excitation of the ligand (the λ_{exc} values are reported in the figure).

orbitals in Figures S1−S12 in the ESI), the values of donor−acceptor distances (R_L, the distance from the unoccupied molecular orbitals centroid to the Eu(III) ion) for IET involving S_1 and T_1 states can be considered the same for each compound (Table 5). For example, Figure S1 shows that the unoccupied molecular orbitals of the *trans-O,O*-[Y(bpcd)$(H_2O)_2]^+$ (**1**) are localized at pyridine group for both S_1 and T_1 states. Thus, R_L is the distance between the center of the pyridine group to Y(III).

As discussed above, the 12 studied isomers were separated into three groups according to their distinct chemical characteristics (i.e., the nature of the heteroaromatic ring). This classification also finds parallelism in the values of the electronic level energy of the ligands involved in the IET

Table 5. Donor−Acceptor Distances R_L (in Å) and Energies of the S_1 and T_1 States (in cm^{-1}) Estimated from TD-DFT Calculations

group	formula (isomer)	R_L	S_1	T_1
I	**1**	3.91	39,412	31,435
	2	3.89	38,185	31,361
	3	3.93	38,546	31,368
	4	3.93	39,818	31,415
II	**5**	4.33	32,445	22,198
	6	4.32	33,271	22,696
	7	4.32	33,391	22,859
	8	4.28	31,818	22,052
III	**9**	5.04	32,087	21,843
	10	5.03	32,136	21,817
	11	5.08	32,000	21,995
	12	5.06	32,235	21,863

process (S_1 and T_1 states; see Table 5): group **I** is composed of complexes **1**−**4** where both S_1 and T_1 are at higher energy (S_1 around 38,900 cm^{-1} and T_1 around 31,400 cm^{-1}) than the complexes in groups **II** (complexes **5**−**8**) and **III** (complexes **9**−**12**). However, the complexes in group **I** present R_L shorter than complexes in groups **II** and **III**. As expected, this finding is connected to the shorter Y−$N_{heterocycle}$ observed in the DFT structures of the [Y(bpcd)$(H_2O)_2]^+$ and [Y(PyC3A)$(H_2O)_2$] complexes (Table 3). The complexes in groups **II** and **III** have similar donor energies (S_1 around 32,400 cm^{-1} and T_1 around 21,100 cm^{-1}), but they are distinguished from each other by the value of R_L (Table 5), where complexes in group **III** present the highest values of R_L among all groups.

The calculated values of λ_M and SOC matrix elements allow estimating the W_{ISC} rates (Table S15) through the Marcus−Levich formalism.[45−47] In addition, from the spin-orbit interaction, the decay lifetimes τ_S and τ_T were estimated (Eq.

https://doi.org/10.1021/acs.inorgchem.2c02330
Inorg. Chem. 2022, 61, 16333−16346

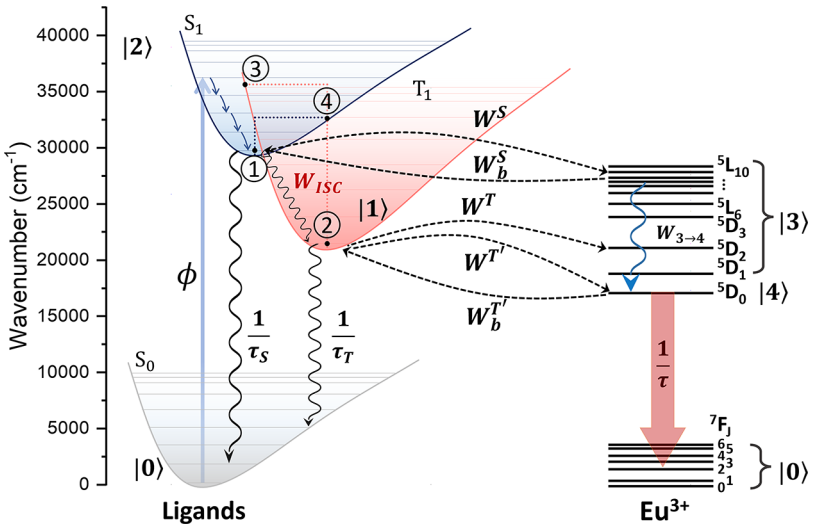

Figure 5. Schematic energy level diagrams for Eu-based complexes in this work. The S_1 and T_1 states for compounds **1′−4′** (group **I**) range from 38,185 to 39,818 cm^{-1} and from 31,361 to 31,435 cm^{-1}, respectively, while those for **5′−12′** (groups **II** and **III**) range from 31,818 to 33,391 cm^{-1} and 22,052 to 22,859 cm^{-1}, respectively (see Table 5). S_0 is the ligand ground level. ϕ is the pumping rate. W_{ISC} is the $S_1 \rightarrow T_1$ ISC rate (Table S15). The blue waved arrow represents the non-radiative decay from higher levels of Eu(III) to the emitting $^5D_0$ while the black ones are the ligand's decay lifetimes (τ_S and τ_T, Table S16). W^S and W^T are the forward energy transfer rates from the S_1 and T_1 states, respectively. Compounds **5′−12′** present significant backward energy transfer rates to the T_1 state (W_b^T). The notation $|N\rangle$ (N = 0, 1, ..., 5) represents levels (or set of levels), and they will be used in the rate equation modeling to determine the theoretical value of the overall quantum yield (ϕ_{ovl}). The points 1, 2, 3, and 4 in the S_1 and T_1 states are related to the Marcus reorganization energies to estimate the ISC rate for each group (see the Supporting Information file).

S12) from the dipole strengths of $S_0 \rightarrow S_1$ and $S_0 \rightarrow T_1$ excitations (S_S and S_T in Table S16).

A trend between the average of experimental $\overline{\phi}_{ovl}$ and computationally obtained W_{ISC}, $1/\tau_S$, and $1/\tau_T$ for the studied compounds can be observed (Figure S15). As these Eu(III) complexes present IET dominated by the T_1 channel, a more effective W_{ISC} is expected to produce a higher ϕ_{ovl}. On the same hand, a smaller $1/\tau_T$ rate induces a higher T_1 population to be transferred to Eu(III), also increasing the overall quantum yield (Figure S15). For these cases, $1/\tau_S$ rates do not follow such trends. These results make clear the importance of the proper computation of W_{ISC}, τ_S, and τ_T quantities, highlighting the importance of the improvements shown in the present work.

Intramolecular Energy Transfer. With the energy values of the S_1 and T_1 states and their donor−acceptor distances (R_L) presented in Table 5, the IET rates can be calculated for each studied compound using eqs 1−5.

Figure 5 shows energy level diagrams that illustrate the ligand-to-Eu(III) energy transfer process. A total of 768 IET rates (64 for each complex, of which 32 for the forward and 32 for backward energy transfer) were obtained with non-zero contributions (see Tables S3−S14). The complete data for forward (W^S and W^T) and backward (W_b^S and W_b^T) IET rates, including the W_{d-d}, W_{d-m}, and W_{ex} mechanisms contributions (eqs 1−3), are presented in Tables S3−S14 while Figure 6 summarizes all IET rates.

Pathways from 1 to 16 (see Tables S3−S14) represent the contributions from S_1, while pathways from 17 to 32 represent the T_1 contributions. W^S and W^T are the sum over all forward pathways (ligand-to-Eu(III)) while W_b^S and W_b^T are the rates for the backward ones (Eu(III)-to-ligand).

The IET results indicate that the channel $T_1 \rightarrow$ Eu(III) is the most effective energy transfer channel for all complexes. For group **I**, pathway 29 (from T_1 to $^7F_1 \rightarrow {}^5G_2$) has the highest forward IET rate, the exchange mechanism (W_{ex}) being the dominating one in the overall IET process. Also, the backward IET rates (from Eu(III) levels to T_1) can be neglected due to a high energy barrier involved (large values of $|\Delta|$). Groups **II** and **III** have the forward rate dominated by pathway 18 (from T_1 to $^7F_0 \rightarrow {}^5D_1$, also governed by the exchange mechanism) and present a considerable W_b^T rate dominated by pathway 29 (from $^7F_1 \rightarrow {}^5G_2$ to T_1). Thus, a consequence of these energies differences in the donor states, particularly regarding the T_1 states, is reflected in the backward energy transfer, where the complexes in group **I** do not have a significant rate while groups **II** and **III** do (W_b^T is around one order of magnitude lower than W^T); see Figure 6. Compounds in Groups **II** and **III** also have a great contribution to the energy transfer directly to the Eu(III) $^5D_0$ emitting level (sum of pathways 17 and 23, represented by the quantity $W^{T\prime}$), which is a reflection of the $^7F_1$ participation in the IET process.[110]

Rate Equations and Overall Quantum Yield. Based on schematic energy level diagrams in Figure 5, the population kinetics can be described by the following general rate equations model for all complexes:

ODE	Level	
$\frac{dP_0}{dt} = -\phi P_0 + \frac{1}{\tau_S}P_2 + \frac{1}{\tau_T}P_1 + \frac{1}{\tau}P_4$	Ground-level	(8)
$\frac{dP_1}{dt} = -\left(\frac{1}{\tau_T} + W^T + W^{T'}\right)P_1 + W_{ISC}P_2 + W_b^T P_3 + W_b^{T'}P_4$	T_1	(9)
$\frac{dP_2}{dt} = -\left(\frac{1}{\tau_S} + W^S + W_{ISC}\right)P_2 + W_b^S P_3 + \phi P_0$	S_1	(10)
$\frac{dP_3}{dt} = -(W_b^S + W_b^T + W_{3\to4})P_3 + W^S P_2 + W^T P_1$	$^5D_1$to$^5L_{10}$	(11)
$\frac{dP_4}{dt} = -\left(\frac{1}{\tau} + W_b^{T'}\right)P_4 + W^{T'}P_1 + W_{3\to4}P_3$	$^5D_0$	(12)

with P_N representing the population of the $|N\rangle$ level as depicted in Figure 5. τ_S, τ_T, and τ are the decay lifetimes of the

https://doi.org/10.1021/acs.inorgchem.2c02330
Inorg. Chem. 2022, 61, 16333−16346

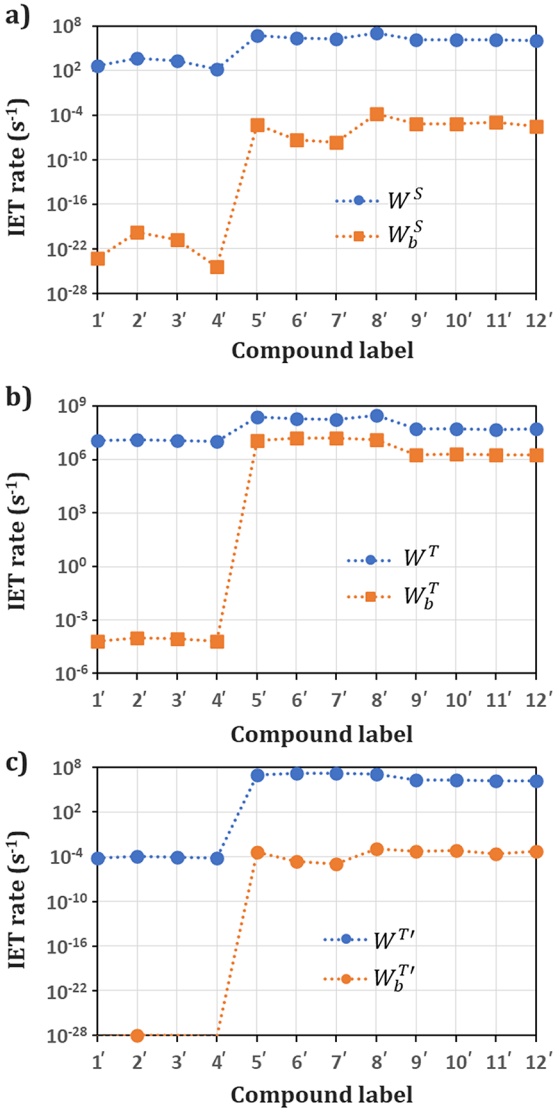

Figure 6. IET rates involving S_1 (a) and T_1 (b, c) states. Involvement of the $^5D_0$ level is reported in (c). The blue circles represent forward rates (W^S, W^T, and $W^{T\prime}$) and the orange squares the backward rates (W_b^S, W_b^T, and $W_b^{T\prime}$). With exception of W_b^T for groups **II** and **III** (compounds from **5′** to **12′**), backward IET rates can be neglected in the rate equation model.

S_1, T_1, and $^5D_0$ levels. The values of these quantities for Ln-based complexes range from 10^{-9} to 10^{-6} s for τ_S, 10^{-6} to 10^{-3} s for τ_T, and $\sim 10^{-3}$ s for τ.[20,78,80]

Table S16 shows the values of τ_S and τ_T obtained from DFT calculations. As stressed before, W_{ISC} is the $S_1 \rightarrow T_1$ ISC rate, and this rate was obtained for one complex of each group due to the complexity of the computational process. Hence, the W_{ISC} for isomers **1′**, **5′**, and **11′** were considered as representative examples of their respective groups (see Table S15 and related discussions in the Supporting Information file). These values were estimated according to the Marcus–Levich framework.[45−47]

W^T and W^S are the forward ligand-to-Eu(III) energy transfer rates while W_b^T and W_b^S are their respective backward energy transfer (Figure 6).

To obtain estimates of the Eu(III) $^5D_0$ emitting level population, the $^5D_0$ state ($|4\rangle$ in Figure 5) was separated from Eu(III) upper levels (state $|3\rangle$ in Figure 5). Thus, the quantities $W_b^{T\prime}$ and $W^{T\prime}$ represent the backward energy transfer rates involving only the Eu(III) emitting level $^5D_0$ and they are obtained by the sum of pathways 17 and 23 in Tables S3–S14.

The population simulations using eqs 8–12 consider the boundary conditions, which guarantee that the sum of the populations on all energy levels should be constant at any time t.[83,110] Thus, the following relationship must be preserved (eq 13):

$$\sum_N P_N(t) = 1 \tag{13}$$

where $P_N(t)$ is the population of state N at time t ($0 \le t \le t_f$).

Table 6 summarizes all rates used in eqs 8–12. Since all compounds present T_1 above the $^5D_0$ level, the values of $W_b^{T\prime}$ (energy transfer from $^5D_0$ to T_1) are very low and can be neglected. On the other hand, the lower energy position of T_1 provided high values of $W^{T\prime}$ (energy transfer rates from T_1 to $^5D_0$ level) for compounds in groups **II** and **III**. The sensitizing process of the Eu(III) ion for all compounds is via the T_1 state.

Figure S13 shows the transient curves of $^5D_0$ and the ground levels for all 12 complexes. It can be noted that group **I** (complexes **1′**, **2′**, **3′**, and **4′**) has the highest $^5D_0$ populations in comparison to the others. This is related to a higher W_{ISC} rate due to a lower S_1–T_1 energy gap (ΔE_{ST}) and the absence of significant backward energy transfer (W_b^S, W_b^T, and $W_b^{T\prime}$). Despite the complexes in group **I** having shorter donor–acceptor distances (Table 5), they presented relatively low rates among the groups. However, the complexes in group **I**

Table 6. IET Rates (in Units of S^{-1}) Used in eqs 8–12 for each Eu(III) Complex

group	isomer	W^S	W_b^S	W^T	$W^{T\prime}$	W_b^T	$W_b^{T\prime}$
I	**1′**	3.9×10^2	10^{-24}	1.2×10^7	9.6×10^1	6.1×10^{-5}	10^{-29}
	2′	4.5×10^3	10^{-20}	1.3×10^7	1.2×10^2	1.0×10^{-4}	10^{-28}
	3′	2.0×10^3	10^{-21}	1.2×10^7	1.1×10^2	8.5×10^{-5}	10^{-29}
	4′	1.6×10^2	10^{-25}	1.1×10^7	9.4×10^1	6.5×10^{-5}	10^{-29}
II	**5′**	5.1×10^6	4.8×10^{-6}	2.5×10^8	4.1×10^7	1.2×10^7	4.1×10^{-4}
	6′	2.2×10^6	5.0×10^{-8}	2.0×10^8	2.8×10^7	1.6×10^7	2.6×10^{-5}
	7′	1.9×10^6	2.4×10^{-8}	1.8×10^8	2.3×10^7	1.7×10^7	1.0×10^{-5}
	8′	1.0×10^7	1.6×10^{-4}	3.0×10^8	5.2×10^7	1.3×10^7	1.1×10^{-3}
III	**9′**	1.4×10^6	6.9×10^{-6}	5.5×10^7	1.0×10^7	2.0×10^6	5.7×10^{-4}
	10′	1.4×10^6	6.7×10^{-6}	5.6×10^7	1.1×10^7	2.0×10^6	6.7×10^{-4}
	11′	1.5×10^6	1.2×10^{-5}	4.8×10^7	8.3×10^6	1.9×10^6	2.3×10^{-4}
	12′	1.2×10^6	3.2×10^{-6}	5.2×10^7	9.6×10^6	1.9×10^6	4.9×10^{-4}

https://doi.org/10.1021/acs.inorgchem.2c02330
Inorg. Chem. 2022, 61, 16333−16346

presented very high energies of the T_1 state (~31,300 cm^{-1}), and this interesting condition allows the uncommon $T_1 \rightarrow [^7F_1 \rightarrow {}^5G_2]$ pathway to be the dominating route (see pathway 29 in Tables S3–S5, and S6) and suppressing the Eu-to-ligand backward transfer. On the other hand, the complexes in groups **II** and **III** presented higher W^T rates (also the backward ones) due to T_1 lower energies (~22,000 cm^{-1}) being in good resonance with the $^5D_1$ level (see pathway 18 in Tables S7–S14).

With the values of populations in the steady-state regime (i.e., the $^5D_0$ and ground-level populations at $t > 2$ ms in Figure S13, P_4 and P_0 respectively), the pumping rate, and radiative rates (Table S1), we obtain the theoretical value of the overall quantum yield (ϕ_{ovl}, eq 7). All these values are summarized in Table 7.

Table 7. Populations of the $^5D_0$ (P_4) and Ground (P_0) Levels (Unitless), Pumping (ϕ), and Radiative (A_{rad}, Table S1) rates (in Units of S^{-1}), and the Overall Quantum Yield ϕ_{ovl} (in %) for Each Eu(III) Complex

group	isomer	P_4	P_0	ϕ	A_{rad}	ϕ_{ovl}
I	1′	3.0×10^{-2}	0.969	128.2	152.6	3.7
	2′	3.1×10^{-2}	0.968	132.4	188.4	4.6
	3′	3.3×10^{-2}	0.967	131.1	250.2	6.5
	4′	3.2×10^{-2}	0.968	126.9	207.9	5.4
II	5′	3.8×10^{-2}	0.962	155.8	207.1	5.2
	6′	3.6×10^{-2}	0.964	151.9	204.4	5.0
	7′	3.6×10^{-2}	0.964	151.4	179.3	4.4
	8′	4.3×10^{-2}	0.957	158.8	120.4	3.4
III	9′	6.9×10^{-3}	0.993	157.5	132.1	0.6
	10′	1.1×10^{-2}	0.989	157.3	186.4	1.4
	11′	2.2×10^{-2}	0.978	157.9	263.7	3.7
	12′	8.3×10^{-3}	0.992	156.8	236.2	1.3

It is important to mention that the ϕ_{ovl} value, in downconversion systems, is independent of the excitation power density since if ϕ(the pumping rate) is n-fold increased, the emitting level population P_4 increases while the ground state is more depleted P_0, but the ratio P_4/P_0 is also n-fold increased. In other words, the ϕ value in the rate equation model does not affect the ϕ_{ovl} calculations.[14]

It can be noted that the compounds in group **I** present higher values of theoretical ϕ_{ovl}, as compound **3′** reaches ϕ_{ovl} = 6.5%. On the other hand, compounds **9′** and **10′** have lower values of ϕ_{ovl} among all compounds due to a low radiative rate (A_{rad}) and $^5D_0$ population (P_4), quantities ascribed to the small values of Ω_λ (mainly the Ω_2, Table S1) and high backward IET rates, respectively. These results are in complete agreement with those determined experimentally for complexes **9′** and **10′** (Table 4). As for the values of the ϕ_{ovl} for the different complexes, we also noticed a good agreement between theoretical and experimental data (see Tables 4 and 7), which confirms the effectiveness of the theoretical modeling without the inclusion of experimental data. A question can be raised regarding whether a better luminescent performance of these compounds could be obtained in the direct excitation of the Eu^{3+} levels (e.g., $^5D_0$ and $^5D_1$). Of course, this avoids non-radiative losses in the process and the ϕ_{ovl} values tend to ϕ_{int}. However, this kind of excitation involves a drastic decrease by order of magnitudes of the molar absorption extinction coefficient ε. In this way, the brightness ($B = \varepsilon \cdot \phi_{ovl}$) is lower in comparison to the excitation through singlet states of the ligands. While ϕ_{ovl} varies between 0 and 1, ε may vary by orders of magnitude. Therefore, it is convenient to optimize energy transfer processes beneficially for the sake of higher brightness.

CONCLUSIONS

In the present work, we have theoretically analyzed 12 Eu(III)-based complexes (all the possible geometric isomers were considered) with the general formula $[Eu(L)(H_2O)_2]^+$ (where L = $bpcd^{2-}$; $bQcd^{2-}$and $biso Qcd^{2-}$) and $Eu(L)(H_2O)_2$ (where L = $PyC3A^{3-}$; $QC3A^{3-}$ and $isoQC3A^{3-}$). TD-DFT calculations revealed the ligand excited donor states and the donor–acceptor distance (R_L). Thus, a total of 768 Ligand↔Eu(III) IET rates were calculated considering the transition of both S_1 and T_1 as donor states (localized in the ligands) and 16 acceptors, involving $^7F_0$ and $^7F_1$ as initial states and $^5D_0$, $^5D_1$, $^5D_2$, $^5D_3$, $^5L_6$, $^5L_7$, $^5G_2$, $^5G_3$, $^5G_4$, $^5G_6$, $^5D_4$, $^5G_5$, $^5L_8$, $^5D_4$, $^5L_9$, and $^5L_{10}$ as final states. The IET rates are affected by (i) donor–acceptor distances (R_L); (ii) the donor (S_1 and T_1) state energy position; and (iii) selection rules on J quantum numbers ($|J - J'| \leq \lambda \leq J + J'$ for dipolar and $\Delta J = J - J' = 0, \pm 1$ for exchange mechanisms). Once (i) and (ii) are associated with the donor excited states, good theoretical treatment is necessary for an appropriate description of IET rates and, therefore, a rate equation model, which enables the prediction of the emitting level population. The energy transfer process for all studied compounds is dominated via the T_1 state, with W^T in some cases more than 10^4 times higher than W^S (compounds **1′** and **4′**, Figure 6). The reason for the higher efficiency of the sensitization process (η_{sens}), around 60–65% in the case of the complexes of group **I** is connected to a shorter R_L combined with a high ISC rates (W_{ISC}) and a negligible backward energy transfer from Eu(III) to S_1 and T_1 level of the ligands. On the contrary, the worst sensitization efficiency (around 25%) recorded in the case of group **II** and **III** complexes (in particular for $[Eu(biso Qcd)(H_2O)_2]^+$, isomers **9′** and **10′**) seems to be due to a significant rate of the Eu(III)-to-T_1 backward energy transfer process ($W_b^T \approx 2 \times 10^6$ s^{-1}) to a lower W_{ISC} and to a larger R_L. To sum up, the forward IET mechanisms mainly involve the Eu(III) $^5G_2$ level for the compounds of the group **I** and $^5D_1$ and $^5D_0$ levels for the compounds of groups **II** and **III**. The backward IET process, significant only for these last complexes, mainly involves the $^5G_2$ level. All the IET processes are dominated by the exchange mechanism.

For the first time, theoretical overall quantum yields (ϕ_{ovl}) were calculated without the introduction of experimental parameters (e.g., decay lifetimes, Judd–Ofelt parameters, energy levels). This was achieved using a blend of DFT, Judd–Ofelt theory, IET theory (including calculated ISC from SOC-TD-DFT), and rate equation modeling. The present work represents a milestone in a detailed description of the luminescence properties of Ln-based chelates. Such a combined experimental/computational study provides deep knowledge of all the variables governing the IET mechanism, and we believe that its extension to other luminescent Ln(III) complexes can make easier the design of new and ever more efficient chromophoric antennae to sensitize the Ln(III) luminescence.

https://doi.org/10.1021/acs.inorgchem.2c02330
Inorg. Chem. 2022, 61, 16333–16346

■ ASSOCIATED CONTENT

Supporting Information

The Supporting Information is available free of charge at https://pubs.acs.org/doi/10.1021/acs.inorgchem.2c02330.

Calculation of the intensity parameters and radiative rates, the matrix elements, the IET and ISC rates, and the decay lifetimes of S_1 and T_1 states; pictures of the molecular orbitals composition of S_1 and T_1 states; and luminescence emission spectra for the calculation of the experimental quantum yields (PDF)

■ AUTHOR INFORMATION

Corresponding Authors

Albano N. Carneiro Neto − *Physics Department and CICECO-Aveiro Institute of Materials, University of Aveiro, 3810-193 Aveiro, Portugal;* orcid.org/0000-0003-2432-0992; Email: albanoneto@ua.pt

Andrea Melchior − *Dipartimento Politecnico di Ingegneria e Architettura, Laboratorio di Tecnologie Chimiche, University of Udine, 33100 Udine, Italy;* orcid.org/0000-0002-5265-1396; Email: andrea.melchior@uniud.it

Fabio Piccinelli − *Luminescent Materials Laboratory, Department of Biotechnology, University of Verona and INSTM, UdR Verona, 37134 Verona, Italy;* orcid.org/0000-0003-0349-1960; Email: fabio.piccinelli@univr.it

Authors

Renaldo T.MouraJr − *Department of Chemistry and Physics, Federal University of Paraíba, 58397-000 Areia, Brazil; Department of Chemistry, Southern Methodist University, Dallas, Texas 75275-0314, United States*

Luís D. Carlos − *Physics Department and CICECO-Aveiro Institute of Materials, University of Aveiro, 3810-193 Aveiro, Portugal;* orcid.org/0000-0003-4747-6535

Oscar L. Malta − *Department of Fundamental Chemistry, Federal University of Pernambuco, 50740-560 Recife, Brazil*

Martina Sanadar − *Dipartimento Politecnico di Ingegneria e Architettura, Laboratorio di Tecnologie Chimiche, University of Udine, 33100 Udine, Italy*

Elfi Kraka − *Department of Chemistry, Southern Methodist University, Dallas, Texas 75275-0314, United States*

Silvia Ruggieri − *Luminescent Materials Laboratory, Department of Biotechnology, University of Verona and INSTM, UdR Verona, 37134 Verona, Italy;* orcid.org/0000-0002-2849-0449

Marco Bettinelli − *Luminescent Materials Laboratory, Department of Biotechnology, University of Verona and INSTM, UdR Verona, 37134 Verona, Italy;* orcid.org/0000-0002-1271-4241

Complete contact information is available at: https://pubs.acs.org/10.1021/acs.inorgchem.2c02330

Author Contributions

The manuscript was written through contributions of all authors. All authors have given approval to the final version of the manuscript.

Notes

The authors declare no competing financial interest.

■ ACKNOWLEDGMENTS

This work was developed within the scope of the projects CICECO-Aveiro Institute of Materials, UIDB/50011/2020, UIDP/50011/2020, and LA/P/0006/2020, and The Shape of Water (PTDC/NAN-PRO/3881/2020) financed by national funds through the FCT/MCTES (PIDDAC). F.P., A.M., M.S., S.R., and M.B. thank the Italian Ministry of University and Research for the received funds in the frame of PRIN (Progetti di Ricerca di Rilevante Interesse Nazionale) project "CHIR-ALAB," Grant No. 20172M3K5N). Also, COST Action CA18202, NECTAR—Network for Equilibria and Chemical Thermodynamics Advanced Research, supported by COST (European Cooperation in Science and Technology), is acknowledged. R.T.M., Jr. and E.K. thank SMU's Center for Scientific Computing for providing generous computational resources. This work was financially supported by the National Science Foundation (Grant CHE 2102461).

■ REFERENCES

(1) Wong, K.-L.; Bünzli, J.-C. G.; Tanner, P. A. Quantum Yield and Brightness. *J. Lumin.* **2020**, *224*, No. 117256.

(2) Bünzli, J.-C. G.; Piguet, C. Taking Advantage of Luminescent Lanthanide Ions. *Chem. Soc. Rev.* **2005**, *34*, 1048.

(3) Hemmilä, I.; Laitala, V. Progress in Lanthanides as Luminescent Probes. *J. Fluoresc.* **2005**, *15*, 529−542.

(4) New, E. J.; Parker, D.; Smith, D. G.; Walton, J. W. Development of Responsive Lanthanide Probes for Cellular Applications. *Curr. Opin. Chem. Biol.* **2010**, *14*, 238−246.

(5) Tsukube, H.; Shinoda, S. Lanthanide Complexes in Molecular Recognition and Chirality Sensing of Biological Substrates. *Chem. Rev.* **2002**, *102*, 2389−2404.

(6) Liu, Z.; He, W.; Guo, Z. Metal Coordination in Photo-luminescent Sensing. *Chem. Soc. Rev.* **2013**, *42*, 1568.

(7) Piccinelli, F.; Leonzio, M.; Bettinelli, M.; Monari, M.; Grazioli, C.; Melchior, A.; Tolazzi, M. Tuning of the Sensing Properties of Luminescent Eu^{3+} Complexes towards the Nitrate Anion. *Dalton Trans.* **2016**, *45*, 3310−3318.

(8) Piccinelli, F.; Leonzio, M.; Bettinelli, M.; Melchior, A.; Faura, G.; Tolazzi, M. Luminescent Eu^{3+}Complexes in Acetonitrile Solution: Anion Sensing and Effect of Water on the Speciation. *Inorg. Chim. Acta* **2016**, *453*, 751−756.

(9) Piccinelli, F.; Melchior, A.; Speghini, A.; Monari, M.; Tolazzi, M.; Bettinelli, M. Europium (III) Complexes with New N-Donor Ligand: A Comparative Study in Solid State and Solution. *Polyhedron* **2013**, *57*, 30−38.

(10) De Rosa, C.; Melchior, A.; Sanadar, M.; Tolazzi, M.; Duerkop, A.; Piccinelli, F. Isoquinoline-Based Eu(Iii) Luminescent Probes for Citrate Sensing in Complex Matrix. *Dalton Trans.* **2021**, *50*, 4700−4712.

(11) De Rosa, C.; Melchior, A.; Sanadar, M.; Tolazzi, M.; Giorgetti, A.; Ribeiro, R. P.; Nardon, C.; Piccinelli, F. Effect of the Heteroaromatic Antenna on the Binding of Chiral Eu(III) Complexes to Bovine Serum Albumin. *Inorg. Chem.* **2020**, *59*, 12564−12577.

(12) Piccinelli, F.; De Rosa, C.; Melchior, A.; Faura, G.; Tolazzi, M.; Bettinelli, M. Eu(Iii) and Tb(Iii) Complexes of 6-Fold Coordinating Ligands Showing High Affinity for the Hydrogen Carbonate Ion: A Spectroscopic and Thermodynamic Study. *Dalton Trans.* **2019**, *48*, 1202−1216.

(13) Leonzio, M.; Melchior, A.; Faura, G.; Tolazzi, M.; Bettinelli, M.; Zinna, F.; Arrico, L.; Di Bari, L.; Piccinelli, F. A Chiral Lactate Reporter Based on Total and Circularly Polarized Tb(Iii) Luminescence. *New J. Chem.* **2018**, *42*, 7931−7939.

(14) Ramalho, J. F. C. B.; Carneiro Neto, A. N.; Carlos, L. D.; André, P. S.; Ferreira, R. A. S.Lanthanides for the New Generation of Optical Sensing and Internet of Things. In *Handbook on the Physics and Chemistry of Rare Earths*; Bünzli, J.-C. G.; Pecharsky, V. K., Eds.; Elsevier B.V, 2022. DOI: 10.1016/bs.hpcre.2021.12.001.

(15) Valentine, A. J. S.; Li, X. Intersystem Crossings in Late-Row Elements: A Perspective. *J. Phys. Chem. Lett.* **2022**, *13*, 3039−3046.

(16) Weber, M. J. Radiative and Multiphonon Relaxation of Rare-Earth Ions in Y_2O_3. *Phys. Rev.* **1968**, *171*, 283−291.
(17) van Dijk, J. M. F.; Schuurmans, M. F. H. On the Nonradiative and Radiative Decay Rates and a Modified Exponential Energy Gap Law for 4*f*−4*f* Transitions in Rare-earth Ions. *J. Chem. Phys.* **1983**, *78*, 5317−5323.
(18) Güdel, H. U.; Pollnau, M. Near-Infrared to Visible Photon Upconversion Processes in Lanthanide Doped Chloride, Bromide and Iodide Lattices. *J. Alloys Compd.* **2000**, *303*−*304*, 307−315.
(19) Dexter, D. L. A Theory of Sensitized Luminescence in Solids. *J. Chem. Phys.* **1953**, *21*, 836−850.
(20) Carneiro Neto, A. N.; Teotonio, E. E. S.; de Sá, G. F.; Brito, H. F.; Legendziewicz, J.; Carlos, L. D.; Felinto, M. C. F. C.; Gawryszewska, P.; Moura, Jr., R. T.; Longo, R. L.; Faustino, W. M.; Malta, O. L.Modeling Intramolecular Energy Transfer in Lanthanide Chelates: A Critical Review and Recent Advances. In *Handbook on the Physics and Chemistry of Rare Earths, volume 56*; Bünzli, J.-C. G.; Pecharsky, V. K., Eds.; Elsevier, 2019; pp. 55−162. DOI: 10.1016/bs.hpcre.2019.08.001.
(21) Bispo-Jr, A. G.; Mazali, I. O.; Sigoli, F. A. Sensitization of Lanthanide Complexes through Direct Spin-Forbidden Singlet → Triplet Excitation. *Phys. Chem. Chem. Phys.* **2022**, *24*, 13565−13570.
(22) Van Lenthe, E.; Baerends, E. J.; Snijders, J. G. Relativistic Total Energy Using Regular Approximations. *J. Chem. Phys.* **1994**, *101*, 9783−9792.
(23) Van Lenthe, E.; Snijders, J. G.; Baerends, E. J. The Zero-Order Regular Approximation for Relativistic Effects: The Effect of Spin-Orbit Coupling in Closed Shell Molecules. *J. Chem. Phys.* **1996**, *105*, 6505−6516.
(24) Douglas, M.; Kroll, N. M. Quantum Electrodynamical Corrections to the Fine Structure of Helium. *Ann. Phys.* **1974**, *82*, 89−155.
(25) Hess, B. A. Applicability of the No-Pair Equation with Free-Particle Projection Operators to Atomic and Molecular Structure Calculations. *Phys. Rev. A* **1985**, *32*, 756−763.
(26) Dyall, K. G. Interfacing Relativistic and Nonrelativistic Methods. I. Normalized Elimination of the Small Component in the Modified Dirac Equation. *J. Chem. Phys.* **1997**, *106*, 9618−9626.
(27) Makoś, M. Z.; Zou, W.; Freindorf, M.; Kraka, E. Metal−Ring Interactions in Actinide Sandwich Compounds: A Combined Normalized Elimination of the Small Component and Local Vibrational Mode Study. *Mol. Phys.* **2020**, *118*, No. e1768314.
(28) Cremer, D.; Zou, W.; Filatov, M. Dirac-exact Relativistic Methods: The Normalized Elimination of the Small Component Method. *WIREs Comput. Mol. Sci.* **2014**, *4*, 436−467.
(29) Zou, W.; Filatov, M.; Cremer, D. Analytical Energy Gradient for the Two-Component Normalized Elimination of the Small Component Method. *J. Chem. Phys.* **2015**, *142*, 214106.
(30) Yoshizawa, T.; Zou, W.; Cremer, D. Calculations of Electric Dipole Moments and Static Dipole Polarizabilities Based on the Two-Component Normalized Elimination of the Small Component Method. *J. Chem. Phys.* **2016**, *145*, 184104.
(31) Costa Peluzo, B. M. T.; Kraka, E. Uranium: The Nuclear Fuel Cycle and Beyond. *Int. J. Mol. Sci.* **2022**, *23*, 4655.
(32) Mori, K.; Goumans, T. P. M.; van Lenthe, E.; Wang, F. Predicting Phosphorescent Lifetimes and Zero-Field Splitting of Organometallic Complexes with Time-Dependent Density Functional Theory Including Spin−Orbit Coupling. *Phys. Chem. Chem. Phys.* **2014**, *16*, 14523−14530.
(33) Brédas, J. L.; Beljonne, D.; Coropceanu, V.; Cornil, J. Charge-Transfer and Energy-Transfer Processes in π-Conjugated Oligomers and Polymers: A Molecular Picture. *Chem. Rev.* **2004**, *104*, 4971−5004.
(34) Georgieva, I.; Zahariev, T.; Aquino, A. J. A.; Trendafilova, N.; Lischka, H. Energy Transfer Mechanism in Luminescence Eu(III) and Tb(III) Complexes of Coumarin-3-Carboxylic Acid: A Theoretical Study. *Spectrochim. Acta, Part A* **2020**, *240*, No. 118591.
(35) Leonzio, M.; Melchior, A.; Faura, G.; Tolazzi, M.; Zinna, F.; Di Bari, L.; Piccinelli, F. Strongly Circularly Polarized Emission from Water-Soluble Eu(III)- and Tb(III)-Based Complexes: A Structural and Spectroscopic Study. *Inorg. Chem.* **2017**, *56*, 4413−4421.
(36) Frisch, M. J.; Trucks, G. W.; Schlegel, H. B.; Scuseria, G. E.; Robb, M. A.; Cheeseman, J. R.; Scalmani, G.; Barone, V.; Petersson, G. A.; Nakatsuji, H.; Li, X.; Caricato, M.; Marenich, A. V.; Bloino, J.; Janesko, B. G.; Gomperts, R.; Mennucci, B.; Hratchian, H. P.; Ortiz, J. V.; Izmaylov, A. F.; Sonnenberg, J. L.; Williams-Young, D.; Ding, F.; Lipparini, F.; Egidi, F.; Goings, J.; Peng, B.; Petrone, A.; Henderson, T.; Ranasinghe, D.; Zakrzewski, V. G.; Gao, J.; Rega, N.; Zheng, G.; Liang, W.; Hada, M.; Ehara, M.; Toyota, K.; Fukuda, R.; Hasegawa, J.; Ishida, M.; Nakajima, T.; Honda, Y.; Kitao, O.; Nakai, H.; Vreven, T.; Throssell, K.; Montgomery, J. A. J.; Peralta, J. E.; Ogliaro, F.; Bearpark, M. J.; Heyd, J. J.; Brothers, E. N.; Kudin, K. N.; Staroverov, V. N.; Keith, T. A.; Kobayashi, R.; Normand, J.; Raghavachari, K.; Rendell, A. P.; Burant, J. C.; Iyengar, S. S.; Tomasi, J.; Cossi, M.; Millam, J. M.; Klene, M.; Adamo, C.; Cammi, R.; Ochterski, J. W.; Martin, R. L.; Morokuma, K.; Farkas, O.; Foresman, J. B.; Fox, D. J.*Gaussian 16, Revision A.03.*; Gaussian, Inc.2016.
(37) Wang, J.; Wang, Y.; Zhang, Z. H.; Zhang, X. D.; Tong, J.; Liu, X. Z.; Liu, X. Y.; Zhang, Y.; Pan, Z. J. Syntheses, Characterization, and Structure Determination of Nine-Coordinate $Na[Y^{III}(Edta)(H_2O)_3]\cdot 5H_2O$ and Eight-Coordinate $Na[Y^{III}(Cydta)(H_2O)_2]\cdot 5H_2O$ Complexes. *J. Struct. Chem.* **2005**, *46*, 895−905.
(38) Mondry, A.; Janicki, R. From Structural Properties of the Eu^{III} Complex with Ethylenediaminetetra(Methylenephosphonic Acid) (H_8EDTMP) towards Biomedical Applications. *Dalton Trans.* **2006**, *39*, 4702−4710.
(39) Wang, J.; Hu, P.; Liu, B.; Xu, R.; Wang, X.; Wang, D.; Zhang, L. Q.; Zhang, X. D. Structural Determination of New Eight-Coordinate $NH_4[Eu^{III}(Cydta)(H_2O)_2]\cdot 4.5H_2O$ and $K_2[Eu_2^{III}(Pdta)_2(H_2O)_2]\cdot 6H_2O$ Complexes. *J. Struct. Chem.* **2011**, *52*, 568−574.
(40) Becke, A. D. Density-Functional Thermochemistry. III. The Role of Exact Exchange. *J. Chem. Phys.* **1993**, *98*, 5648−5652.
(41) Lee, C.; Yang, W.; Parr, R. G. Development of the Colle-Salvetti Correlation-Energy Formula into a Functional of the Electron Density. *Phys. Rev. B* **1988**, *37*, 785−789.
(42) Dolg, M.; Stoll, H.; Preuss, H. Energy-adjusted Ab Initio Pseudopotentials for the Rare Earth Elements. *J. Chem. Phys.* **1989**, *90*, 1730−1734.
(43) Mennucci, B.; Tomasi, J. Continuum Solvation Models: A New Approach to the Problem of Solute's Charge Distribution and Cavity Boundaries. *J. Chem. Phys.* **1997**, *106*, 5151−5158.
(44) Runge, E.; Gross, E. K. U. Density-Functional Theory for Time-Dependent Systems. *Phys. Rev. Lett.* **1984**, *52*, 997−1000.
(45) Marcus, R. A. On the Theory of Oxidation-Reduction Reactions Involving Electron Transfer. I. *J. Chem. Phys.* **1956**, *24*, 966−978.
(46) Marcus, R. A. Electron Transfer Reactions in Chemistry: Theory and Experiment (Nobel Lecture). *Angew. Chem., Int. Ed. Engl.* **1993**, *32*, 1111−1121.
(47) Bixon, M.; Jortner, J. Intramolecular Radiationless Transitions. *J. Chem. Phys.* **1968**, *48*, 715−726.
(48) de Souza, B.; Farias, G.; Neese, F.; Izsák, R. Predicting Phosphorescence Rates of Light Organic Molecules Using Time-Dependent Density Functional Theory and the Path Integral Approach to Dynamics. *J. Chem. Theory Comput.* **2019**, *15*, 1896−1904.
(49) Neese, F. Software update: TheORCAprogram system—Version 5.0. *WIREs Comput. Mol. Sci.* **2022**, *12*, No. e1606.
(50) Weigend, F.; Ahlrichs, R. Balanced Basis Sets of Split Valence, Triple Zeta Valence and Quadruple Zeta Valence Quality for H to Rn: Design and Assessment of Accuracy. *Phys. Chem. Chem. Phys.* **2005**, *7*, 3297.
(51) Pantazis, D. A.; Neese, F. All-Electron Scalar Relativistic Basis Sets for the Lanthanides. *J. Chem. Theory Comput.* **2009**, *5*, 2229−2238.
(52) Weigend, F. Accurate Coulomb-Fitting Basis Sets for H to Rn. *Phys. Chem. Chem. Phys.* **2006**, *8*, 1057.

(53) Neese, F. Efficient and Accurate Approximations to the Molecular Spin-Orbit Coupling Operator and Their Use in Molecular g-Tensor Calculations. *J. Chem. Phys.* **2005**, *122*, No. 034107.
(54) Malta, O. L. Ligand—Rare-Earth Ion Energy Transfer in Coordination Compounds. A Theoretical Approach. *J. Lumin.* **1997**, *71*, 229−236.
(55) Malta, O. L.; Gonçalves e Silva, F. R. A Theoretical Approach to Intramolecular Energy Transfer and Emission Quantum Yields in Coordination Compounds of Rare Earth Ions. *Spectrochim. Acta, Part A* **1998**, *54*, 1593−1599.
(56) Longo, R.; Gonçalves e Silva, F. R.; Malta, O. L. A Theoretical Study of the Energy-Transfer Process in $[Eu\subset bpy.Bpy.Bpy]^{3+}$ Cryptates: A Ligand-to-Metal Charge-Transfer State? *Chem. Phys. Lett.* **2000**, *328*, 67−74.
(57) Malta, O. L. Mechanisms of Non-Radiative Energy Transfer Involving Lanthanide Ions Revisited. *J. Non-Cryst. Solids* **2008**, *354*, 4770−4776.
(58) Judd, B. R. Optical Absorption Intensities of Rare-Earth Ions. *Phys. Rev.* **1962**, *127*, 750−761.
(59) Ofelt, G. S. Intensities of Crystal Spectra of Rare-Earth Ions. *J. Chem. Phys.* **1962**, *37*, 511−520.
(60) Malta, O. L. Theoretical Crystal-Field Parameters for the $YOCl:Eu^{3+}$ System. A Simple Overlap Model. *Chem. Phys. Lett.* **1982**, *88*, 353−356.
(61) Malta, O. L. A Simple Overlap Model in Lanthanide Crystal-Field Theory. *Chem. Phys. Lett.* **1982**, *87*, 27−29.
(62) Moura, R. T., Jr.; Carneiro Neto, A. N.; Aguiar, E. C.; Santos, C. V., Jr.; de Lima, E. M.; Faustino, W. M.; Teotonio, E. E. S.; Brito, H. F.; Felinto, M. C. F. C.; Ferreira, R. A. S.; Carlos, L. D.; Longo, R. L.; Malta, O. L. JOYSpectra: A Web Platform for Luminescence of Lanthanides. *Opt. Mater.: X* **2021**, *11*, No. 100080.
(63) Carnall, W. T.; Crosswhite, H.; Crosswhite, H. M.*Energy Level Structure and Transition Probabilities in the Spectra of the Trivalent Lanthanides in* LaF_3; Argonne National Lab. (ANL): Argonne, IL, United States, 1978. DOI: 10.2172/6417825.
(64) Ofelt, G. S. Structure of the f6 Configuration with Application to Rare-Earth Ions. *J. Chem. Phys.* **1963**, *38*, 2171−2180.
(65) Kasprzycka, E.; Carneiro Neto, A. N.; Trush, V. A.; Jerzykiewicz, L.; Amirkhanov, V. M.; Malta, O. L.; Legendziewicz, J.; Gawryszewska, P. How Minor Structural Changes Generate Major Consequences in Photophysical Properties of RE Coordination Compounds; Resonance Effect, LMCT State. *J. Rare Earths* **2020**, *38*, 552−563.
(66) Edvardsson, S.; Klintenberg, M. Role of the Electrostatic Model in Calculating Rare-Earth Crystal-Field Parameters. *J. Alloys Compd.* **1998**, *275*−*277*, 230−233.
(67) Judd, B. R.*Operator Techniques in Atomic Spectroscopy*; McGraw-Hill Book Company: New York, 1998.
(68) Carneiro Neto, A. N.; Moura, R. T., Jr. Overlap Integrals and Excitation Energies Calculations in Trivalent Lanthanides 4f Orbitals in Pairs Ln-L (L = Ln, N, O, F, P, S, Cl, Se, Br, and I). *Chem. Phys. Lett.* **2020**, *757*, No. 137884.
(69) e Silva, F. R. G.; Malta, O. L. Calculation of the Ligand−Lanthanide Ion Energy Transfer Rate in Coordination Compounds: Contributions of Exchange Interactions. *J. Alloys Compd.* **1997**, *250*, 427−430.
(70) Sato, S.; Wada, M. Relations between Intramolecular Energy Transfer Efficiencies and Triplet State Energies in Rare Earth β-Diketone Chelates. *Bull. Chem. Soc. Jpn.* **1970**, *43*, 1955−1962.
(71) Teotonio, E. E. S.; Brito, H. F.; de Sá, G. F.; Felinto, M. C. F. C.; Santos, R. H. A.; Fuquen, R. M.; Costa, I. F.; Kennedy, A. R.; Gilmore, D.; Faustino, W. M. Structure and Luminescent Investigation of the Ln(III)−β-Diketonate Complexes Containing Tertiary Amides. *Polyhedron* **2012**, *38*, 58−67.
(72) Carneiro Neto, A. N.; Moura, R. T., Jr.; Shyichuk, A.; Paterlini, V.; Piccinelli, F.; Bettinelli, M.; Malta, O. L. Theoretical and Experimental Investigation of the $Tb^{3+} \rightarrow Eu^{3+}$ Energy Transfer Mechanisms in Cubic $A_3Tb_{0.90}Eu_{0.10}(PO_4)_3$ (A = Sr, Ba) Materials. *J. Phys. Chem. C* **2020**, *124*, 10105−10116.
(73) Aquino, L. E. d. N.; Barbosa, G. A.; Ramos, J. d. L.; Giese, S. O. K.; Santana, F. S.; Hughes, D. L.; Nunes, G. G.; Fu, L.; Fang, M.; Poneti, G.; Carneiro Neto, A. N.; Moura, R. T., Jr.; Ferreira, R. A. S.; Carlos, L. D.; Macedo, A. G.; Soares, J. F. Seven-Coordinate Tb^{3+} Complexes with 90% Quantum Yields: High-Performance Examples of Combined Singlet- and Triplet-to-Tb^{3+} Energy-Transfer Pathways. *Inorg. Chem.* **2021**, *60*, 892−907.
(74) Pham, Y. H.; Trush, V. A.; Carneiro Neto, A. N.; Korabik, M.; Sokolnicki, J.; Weselski, M.; Malta, O. L.; Amirkhanov, V. M.; Gawryszewska, P. Lanthanide Complexes with *N*-Phosphorylated Carboxamide as UV Converters with Excellent Emission Quantum Yield and Single-Ion Magnet Behavior. *J. Mater. Chem. C* **2020**, *8*, 9993−10009.
(75) Grant, W. J. C. Role of Rate Equations in the Theory of Luminescent Energy Transfer. *Phys. Rev. B* **1971**, *4*, 648−663.
(76) Butcher, J. C. Numerical Methods for Ordinary Differential Equations in the 20th Century. *J. Comput. Appl. Math* **2000**, *125*, 1−29.
(77) Hairer, E.; Wanner, G.Radau Methods. In *Encyclopedia of Applied and Computational Mathematics*; Engquist, B., Ed.; Springer Berlin Heidelberg: Berlin, Heidelberg, 2015; pp. 1213−1216. DOI: 10.1007/978-3-540-70529-1_139.
(78) Kasprzycka, E.; Carneiro Neto, A. N.; Trush, V. A.; Malta, O. L.; Jerzykiewicz, L.; Amirkhanov, V. M.; Legendziewicz, J.; Gawryszewska, P. Spectroscopic Aspects for the Yb^{3+} Coordination Compound with a Large Energy Gap between the Ligand and Yb^{3+} Excited States. *Spectrochim. Acta, Part A* **2022**, No. 121072.
(79) Fang, M.; Neto, A. N. C.; Fu, L.; Ferreira, R. A. S.; De Zea Bermudez, V.; Carlos, L. D. A Hybrid Materials Approach for Fabricating Efficient WLEDs Based on Di-Ureasils Doped with Carbon Dots and a Europium Complex. *Adv. Mater. Technol.* **2021**, *274*, 2100727.
(80) Carneiro Neto, A. N.; Mamontova, E.; Botas, A. M. P.; Brites, C. D. S.; Ferreira, R. A. S.; Rouquette, J.; Guari, Y.; Larionova, J.; Long, J.; Carlos, L. D. Rationalizing the Thermal Response of Dual-Center Molecular Thermometers: The Example of an Eu/Tb Coordination Complex. *Adv. Opt. Mater.* **2022**, *10*, 2101870.
(81) Ramalho, J. F. C. B.; Dias, L. M. S.; Fu, L.; Botas, A. M. P.; Carlos, L. D.; Carneiro Neto, A. N.; André, P. S.; Ferreira, R. A. S. Customized Luminescent Multiplexed Quick-Response Codes as Reliable Temperature Mobile Optical Sensors for EHealth and Internet of Things. *Adv. Photonics. Res.* **2022**, *3*, 2100206.
(82) Lyubov, D.; Carneiro Neto, A. N.; Fayoumi, A.; Lyssenko, K. A.; Korshunov, V.; Taydakov, I. V.; Salles, F.; Guari, Y.; Larionova, J.; Carlos, L. A. D.; Long, J.; Trifonov, A. Employing Three-Blade Propeller Lanthanide Complexes as Molecular Luminescent Thermometers: Study of the Temperature Sensing through a Concerted Experimental/Theory Approach. *J. Mater. Chem. C* **2022**, 7176.
(83) Carneiro Neto, A. N.; Kasprzycka, E.; Souza, A. S.; Gawryszewska, P.; Suta, M.; Carlos, L. D.; Malta, O. L. On the Long Decay Time of the $^7F_5$ Level of Tb^{3+}. *J. Lumin.* **2022**, *248*, No. 118933.
(84) Brito, H. F.; Malta, O. M. L.; Felinto, M. C. F. C.; Teotonio, E. E. S.Luminescence Phenomena Involving Metal Enolates. In *PATAI'S Chemistry of Functional Groups*; John Wiley & Sons, Ltd: Chichester, UK, 2010. DOI: 10.1002/9780470682531.pat0419.
(85) Bünzli, J.-C. G.; Eliseeva, S. V.Basics of Lanthanide Photophysics. In *Lanthanide Luminescence: Photophysical, Analytical and Biological Aspects, vol 7*; Hänninen, P.; Härmä, H., Eds.; Springer: Berlin, Heidelberg, 2010; pp. 1−45. DOI: 10.1007/4243_2010_3.
(86) Bünzli, J.-C. G. On the Design of Highly Luminescent Lanthanide Complexes. *Coord. Chem. Rev.* **2015**, *293*−*294*, 19−47.
(87) Safdar, M.; Ghazy, A.; Lastusaari, M.; Karppinen, M. Lanthanide-Based Inorganic−Organic Hybrid Materials for Photon-Upconversion. *J. Mater. Chem. C* **2020**, *8*, 6946−6965.
(88) Sen, R.; Paul, S.; Sarkar, A.; Botas, A. M. P.; Carneiro Neto, A. N.; Brandão, P.; Lopes, A. M. L.; Ferreira, R. A. S.; Araújo, J. P.; Lin, Z. A New Series of 3D Lanthanide Phenoxycarboxylates: Synthesis,

Crystal Structure, Magnetism and Photoluminescence Studies. *CrystEngComm* **2021**, *23*, 4143−4151.
(89) Eaton, D. F. Reference Materials for Fluorescence Measurement. *Pure Appl. Chem.* **1988**, *60*, 1107−1114.
(90) Shannon, R. D. Revised Effective Ionic Radii and Systematic Studies of Interatomic Distances in Halides and Chalcogenides. *Acta Crystallogr., Sect. A* **1976**, *32*, 751−767.
(91) Di Bernardo, P.; Melchior, A.; Tolazzi, M.; Zanonato, P. L. Thermodynamics of Lanthanide(III) Complexation in Non-Aqueous Solvents. *Coord. Chem. Rev.* **2012**, *256*, 328−351.
(92) Rayer, A. V.; Sumon, K. Z.; Jaffari, L.; Henni, A. Dissociation Constants (pK_a) of Tertiary and Cyclic Amines: Structural and Temperature Dependences. *J. Chem. Eng. Data* **2014**, *59*, 3805−3813.
(93) Ferreirós-Martínez, R.; Esteban-Gómez, D.; Platas-Iglesias, C.; de Blas, A.; Rodríguez-Blas, T. Zn(Ii), Cd(Ii) and Pb(Ii) Complexation with Pyridinecarboxylate Containing Ligands. *Dalton Trans.* **2008**, *42*, 5754.
(94) Tei, L.; Baranyai, Z.; Gaino, L.; Forgács, A.; Vágner, A.; Botta, M. Thermodynamic Stability, Kinetic Inertness and Relaxometric Properties of Monoamide Derivatives of Lanthanide(Iii) DOTA Complexes. *Dalton Trans.* **2015**, *44*, 5467−5478.
(95) Gale, E. M.; Mukherjee, S.; Liu, C.; Loving, G. S.; Caravan, P. Structure−Redox−Relaxivity Relationships for Redox Responsive Manganese-Based Magnetic Resonance Imaging Probes. *Inorg. Chem.* **2014**, *53*, 10748−10761.
(96) Tanabe, S.; Ohyagi, T.; Soga, N.; Hanada, T. Compositional Dependence of Judd-Ofelt Parameters of Er^{3+} Ions in Alkali-Metal Borate Glasses. *Phys. Rev. B* **1992**, *46*, 3305−3310.
(97) Jørgensen, C. K.; Reisfeld, R. Judd-Ofelt Parameters and Chemical Bonding. *J. Less-Common Met.* **1983**, *93*, 107−112.
(98) Supkowski, R. M.; Horrocks, W. D., Jr. On the Determination of the Number of Water Molecules, q, Coordinated to Europium(III) Ions in Solution from Luminescence Decay Lifetimes. *Inorg. Chim. Acta* **2002**, *340*, 44−48.
(99) Horrocks, W. D., Jr.; Bolender, J. P.; Smith, W. D.; Supkowski, R. M. Photosensitized Near Infrared Luminescence of Ytterbium(III) in Proteins and Complexes Occurs via an Internal Redox Process. *J. Am. Chem. Soc.* **1997**, *119*, 5972−5973.
(100) Horrocks, W. D., Jr.; Sudnick, D. R. Lanthanide Ion Probes of Structure in Biology. Laser-Induced Luminescence Decay Constants Provide a Direct Measure of the Number of Metal-Coordinated Water Molecules. *J. Am. Chem. Soc.* **1979**, *101*, 334−340.
(101) Binnemans, K. Interpretation of Europium(III) Spectra. *Coord. Chem. Rev.* **2015**, *295*, 1−45.
(102) Kariaka, N.; Trush, V. A.; Dyakonenko, V. V.; Shishkina, S. V.; Smola, S. S.; Rusakova, N. V.; Sliva, T. Y.; Gawryszewska, P.; Neto, A. N. C.; Malta, O. L.; Amirkhanov, V. M. New Luminescent Lanthanide Tetrakis-complexes $NEt_4[LnL_4]$ Based on Dimethyl-N-benzoylamidophosphate. *ChemPhysChem* **2022**, *23*, No. e202200129.
(103) Bettinelli, M.; Speghini, A.; Piccinelli, F.; Neto, A. N. C.; Malta, O. L. Luminescence Spectroscopy of Eu^{3+} in $Ca_3Sc_2Si_3O_{12}$. *J. Lumin.* **2011**, *131*, 1026−1028.
(104) Peacock, R. D.The Intensities of Lanthanide f ↔ f Transitions. In *Rare Earths*; Springer Berlin Heidelberg: Berlin, Heidelberg; pp. 83−122. DOI: 10.1007/BFb0116556.
(105) Carlos, L. D.; Videira, A. L. L. Emission Spectra and Local Symmetry of the Eu^{3+} Ion in Polymer Electrolytes. *Phys. Rev. B* **1994**, *49*, 11721−11728.
(106) Malta, O. L.; Azevedo, W. M.; Gouveia, E. A.; de Sá, G. F. On the $^5D_0 \rightarrow {}^7F_0$ Transition of the Eu^{3+} Ion in the $\{(C_4H_9)_4N\}_3Y(NCS)_6$ Host. *J. Lumin.* **1982**, *26*, 337−343.
(107) Hälsä, J.; Porcher, P. Free Ion and Crystal Field Parameters for REOCl:Eu^{3+}. *J. Chem. Phys.* **1981**, *75*, 2108−2117.
(108) Porcher, P.; Caro, P. Crystal Field Parameters for Eu^{3+} in KY_3F_{10}. II. Intensity Parameters. *J. Chem. Phys.* **1978**, *68*, 4176−4182.
(109) Hälsä, J.; Porcher, P. Crystal Field Effects in REOBr:Eu^{3+}. *J. Chem. Phys.* **1982**, *76*, 2790−2797.
(110) Blois, L.; Carneiro Neto, A. N.; Malta, O. L.; Brito, H. F. The Role of the Eu^{3+} $^7F_1$ Level in the Direct Sensitization of the $^5D_0$ Emitting Level through Intramolecular Energy Transfer. *J. Lumin.* **2022**, *247*, No. 118862.